The rice bundle sheath produces reactive oxygen species during high light stress via NADPH oxidase

Haiyan Xiong[1], Lei Hua[1], Yi Shi[2], Kun-Ming Chen[2], Nicholas Smirnoff[3], Johannes Kromdijk[1] and Julian M. Hibberd[1]

[1] Department of Plant Sciences, University of Cambridge, Downing Street, Cambridge CB2 3EA, United Kingdom.

[2] State Key Laboratory of Crop Stress Biology in Arid Area/College of Life Sciences, Northwest A&F University, Yangling, Shaanxi, 712100, China.

[3] College of Life and Environmental Sciences, University of Exeter, EX4 4QD, United Kingdom.

Email addresses:

HX - hx253@cam.ac.uk

LH - lh556@cam.ac.uk

YS - 17749124768@163.com

KC - kunmingchen@nwsuaf.edu.cn

NS - n.smirnoff@exeter.ac.uk

JK - jk417@cam.ac.uk

JMH - jmh65@cam.ac.uk

Running title: High light response of the rice bundle sheath

Keywords: rice; bundle sheath strands; reactive oxygen species; high light; mesophyll

Abstract

When exposed to high light plants produce reactive oxygen species (ROS). In *Arabidopsis thaliana* local accumulation of ROS preferentially takes place in bundle sheath strands, but little is known about how this response takes place. Using rice and the ROS probes diaminobenzidine and 2',7'-dichlorodihydrofluorescein diacetate, we found that after exposure to high light, ROS were produced more rapidly in bundle sheath strands than mesophyll cells. This response was not affected either by CO_2 supply or photorespiration. Consistent with these findings, deep sequencing of mRNA isolated from mesophyll or bundle sheath strands indicated balanced accumulation of transcripts encoding all major components of the photosynthetic apparatus. However, transcripts encoding several isoforms of the superoxide/H_2O_2-producing enzyme NADPH oxidase were more abundant in bundle sheath strands than mesophyll cells. ROS production in bundle sheath strands was reduced by blocking NADPH oxidase activity pharmacologically, but increased when the bundle sheath preferential *RBOHA* isoform of NADPH oxidase was over-expressed. NADPH oxidase mediated accumulation of ROS in the rice bundle sheath was detected in etiolated leaves lacking chlorophyll indicating that high light and NADPH oxidase-dependent ROS production is not dependent on photosynthesis.

Introduction

Under high-light conditions the capacity for light capture during photosynthesis can exceed use. This can lead to damage, generate signals promoting repair, and also initiate responses allowing acclimation (Asada, 1999; Li et al., 2009; Mullineaux et al., 2018). One source of damage is an increase in the production of reactive oxygen species (ROS). For example, oxygen photoreduction, largely at Photosystem I can result in superoxide and hydrogen peroxide. The other source is singlet oxygen which is formed by interaction of oxygen with triplet state chlorophyll in Photosystem II (Noctor and Foyer, 1998; Li et al., 2009; Murchie and Niyogi, 2011). As ROS are potentially harmful, with the ability to damage Fe-S proteins, oxidise amino acid residues and generate further radicals and reactive electrophiles resulting in lipid peroxidation and DNA damage, photosynthetic organisms have evolved a variety of mechanisms to minimize over-excitation of the photosystems. These range from transcriptional responses mediated by retrograde signaling between chloroplast and nucleus (Rossel et al., 2002; Kimura et al., 2003; Kleine et al., 2007; Li et al., 2009; Ruckle et al., 2012; Vogel et al., 2014; Dietz, 2015; Crisp et al., 2017; Mullineaux et al., 2018) to more immediate remodeling of light harvesting structures to dissipate excess excitation energy (Muller, 2001; Ruban, 2016).

Processes that dissipate energy in excess of that used by the photosynthetic electron transport chain are collectively known non-photochemical quenching (NPQ) mechanisms, and their induction is thought to reduce damage to the photosynthetic apparatus caused by synthesis of ROS (Demmig-Adams and Adams, 1992; Muller, 2001). As such, the scavenging/antioxidant network to remove ROS and repair damge is complex (Asada, 1999; Mullineaux et al., 2006; Miller et al., 2010). Notably, although in C_3 species such as *Arabidopsis thaliana*, mesophyll cells contain the majority of chlorophyll in a leaf, after exposure to excess light ROS accumulate preferentially in bundle sheath cells that surround veins (Fryer et al., 2002; Fryer et al., 2003; Mullineaux et al., 2006; Galvez-Valdivieso et al., 2009). ROS have been implicated in rapid systemic signaling responses initiated after various abiotic and biotic stresses including heat, wounding and pathogen attack (Fichman and Mittler, 2020). Such ROS mediated signaling from a locally perturbed leaf can lead to stomatal aperture being altered in distant leaves, is associated with the hormones abscisic and jasmonic acid, and dependent on the plasma membrane localized NADPH oxidase

(Respiratory Burst Oxidase Homolog D (RBOHD) (Devireddy et al., 2018; Devireddy et al., 2020).

In contrast to C_4 species in which the role of the bundle sheath in fixing CO_2 by RuBisCO has been understood for decades (Hatch, 1987), this cell-type is poorly characterized in C_3 species. Whilst the bundle sheath of C_3 plants contains chloroplasts that accumulate starch (Miyake and Maeda, 1976; Kinsman and Pyke, 1998) they are not as numerous as those in the mesophyll and reducing chlorophyll accumulation in these cells has limited impact on photosynthesis (Janacek et al., 2009). Rather, in *A. thaliana* the bundle sheath is thought to be specialized in sulphur metabolism, glucosinolate biosynthesis (Gigolashvili et al., 2007; Koroleva et al., 2010; Aubry et al., 2014) and transport of water and solutes in and out of the leaf (Aubry et al., 2014). In particular, stress responsive activation of aquaporins in bundle-sheath cells are important in hydraulic conductivity of the whole leaf (Shatil-Cohen et al., 2011; Sade et al., 2014; Sadey et al., 2015). Consistent with this, bundle sheath cells more generally have been proposed to play a role in maintaining hydraulic integrity of the xylem (Sage, 2001; Griffiths et al., 2013) and in regulating flux of metabolites in and out of the leaf (Leegood, 2008).

To our knowledge none of these previous studies explain how the bundle sheath of C_3 plants preferentially accumulates ROS. One possibility is that supply of atmospheric CO_2 to cells around the veins is limited and so inorganic carbon present in the transpiration stream provides CO_2 to photosynthesis (Hibberd and Quick, 2002; Brown et al., 2010). If this were the case, when stomata close, provision of CO_2 from veins could slow activity of the Calvin Bassham Benson cycle compared with chlorophyll de-excitation in the light harvesting complexes (Galvez-Valdivieso et al., 2009). Although, proximity of bundle sheath cells to veins could provide an efficient mechanism to initiate systemic acclimation to high-light stress (Mullineaux et al., 2006) the mechanism/s by which ROS accumulate in bundle sheath cells is unclear, and to our knowledge how common this response is beyond *A. thaliana* is not known.

Using rice, we show that ability of the C_3 bundle sheath to preferentially accumulate ROS in response to high light is found in the monocotyledons as well as the dicotyledons. We found no evidence that ROS accumulation in the C_3 bundle sheath was due to limited CO_2 supply, nor to production of H_2O_2 from photorespiration – in fact we detected clear ROS

110 accumulation in bundle sheath cells of C_4 species in which photorespiration is essentially
111 abolished. We also found no evidence for an imbalance between transcript abundance of
112 genes encoding components of light harvesting apparatus and the Calvin Bassham Benson
113 cycle. However, we did find that transcripts encoding NADPH oxidases accumulate
114 preferentially in bundle sheath cells. Pharmacological treatment to block their activity and
115 overexpression reduced and increased accumulation of ROS in the bundle sheath of rice
116 respectively. Although accumulation of ROS in the bundle sheath was strongest in green
117 leaves containing light harvesting apparatus, accumulation was still detected in etiolated
118 leaves.

119 **Results**

120 **Veins and bundle sheath cells of rice preferentially accumulate reactive oxygen**
121 **species in response to high light**

122 Rice leaves were exposed for 90 minutes to a light intensity tenfold higher than that used
123 for growth. As expected, this led to a rapid and sustained reduction in the chlorophyll
124 fluorescence parameters Fv'/Fm' and Fq'/Fm' (Figure 1A&B) that report the maximum
125 efficiency of Photosystem II and its operating efficiency respectively. Over the same period,
126 photochemical quenching first decreased and then recovered slowly, whilst non-
127 photochemical quenching increased steadily (Figure 1C). Representative images of Fv'/Fm'
128 over this time-course indicated that responses of the photosynthetic apparatus to high light
129 were relatively homogenous across the leaf (Figure 1D). Together, these data show that
130 subjecting rice leaves to excess light led to the expected response of Photosystem II
131 efficiency.

132 We next tested whether preferential accumulation of ROS in bundle sheath cells as
133 reported in *A. thaliana* (Fryer et al., 2002; Fryer et al., 2003; Galvez-Valdivieso et al., 2009)
134 was detectable in rice. The cytochemical dye 3, 3-diaminobenzidine (DAB) is routinely used
135 to detect H_2O_2. It reacts with H_2O_2 to form a brown polymerization product, the reaction
136 being accelerated by peroxidase (Thordal-Christensen et al., 1997). In contrast to the
137 relatively homogenous alterations to chlorophyll fluorescence parameters reporting on the
138 activity of Photosystem II (Figure 1D), preferential accumulation of the DAB polymerization
139 product (hereafter referred to as DAB) was detected in patches of longitudinal files of cells
140 after five minutes, and then in almost all files of these cells after thirty minutes of exposure
141 to high light (Figure 1E). Paradermal sections from leaves were generated in order to
142 determine the specific cell types involved, and this showed that thirty minutes after exposure
143 to high light the strongest DAB signal was associated with veins and bundle sheath cells
144 (Figure 1F). We refer to these cells as bundle sheath strands (BSS) as they include both the
145 bundle sheath and the vascular strands. Quantitation of this signal from multiple sections
146 confirmed that bundle sheath strands consistently accumulated more DAB than the
147 surrounding mesophyll cells (Figure 1G) and more dense sampling indicated that the
148 increase in DAB was first detectable ten minutes after the transfer to high light (Figure
149 S1A&B). From around fifteen minutes after the treatment, DAB also increased in mesophyll

150 cells, but the signal was always stronger in bundle sheath strands (Figure S1A&B). We used
151 the ROS sensitive fluorescent dye 2',7'-dichlorodihydrofluorescein diacetate (H_2DCFDA) to
152 provide independent evidence that rice bundle sheath strands were particularly responsive
153 to high light. In the presence of peroxidases and radicals generated by ROS in living plant
154 cells, H_2DCFDA produces highly fluorescent 2',7'-dichlorofluorescein (DCF) (Winterbourn,
155 2014). Consistent with the results obtained with DAB, when H_2DCFDA was supplied to rice
156 leaves, high light led to brighter green fluorescence in bundle sheath strands than
157 neighbouring cells (Figure S2A). To exclude the possibility that H_2DCFDA had not uniformly
158 penetrated mesophyll cells, we supplied a subset of leaves with exogenous H_2O_2 (Figure
159 S2B). This led to DCF fluorescence from both mesophyll as well as bundle sheath strands
160 indicating that the increased signal in the bundle sheath after exposure to high light was
161 unlikely to be an artefact of incomplete transport into all cells of the leaf (Figure S2B).
162 Localised staining also rules out direct dye oxidation by light (Winterbourn, 2014). We
163 conclude that as with *A. thaliana*, veins and bundle sheath cells of rice preferentially
164 accumulate ROS in response to high light treatment and thus that this may be a property
165 found in both dicotyledons and monocotyledons.
166

167 **Over-capacity in light harvesting compared with Calvin-Benson-Bassham cycle**
168 **capacity is unlikely the cause of DAB accumulation in rice bundle sheath strands**

169 Excess excitation energy that cannot be fully utilized by carbon assimilation and other
170 metabolic processes in chloroplasts gives rise to ROS during exposure to high light intensity
171 (Fryer et al., 2003; Apel and Hirt, 2004; Bechtold et al., 2008). The greater production of
172 ROS in the BSS compared with mesophyll cells implies a greater capacity for ROS
173 production or a limitation imposed by CO_2 assimilation rate. As bundle sheath strands are
174 distant from stomata, and in contact with fewer intercellular air spaces than mesophyll cells,
175 we reasoned that they may be CO_2 limited. Thus, flux through the Calvin-Benson-Bassham
176 cycle may be constrained compared with activity of the photosynthetic electron transport
177 chain. If this were the case, reducing and increasing the CO_2 concentration around leaves
178 would be expected to respectively enhance and repress preferential DAB staining in bundle
179 sheath strands. However, we found evidence for neither. High light exposure at 200 ppm
180 [CO_2], which would restrict activity of the Calvin Benson Bassham cycle, led to preferential

181 but similar DAB staining in the bundle sheath strands and 2000 ppm [CO_2], which should
182 saturate RuBisCO in bundle sheath as well as mesophyll cells, failed to abolish the
183 preferential DAB staining in these cells (Figure 2A&B).

184 The oxygenation reaction of RuBisCO requires the photorespiratory pathway to detoxify
185 the initial product phosphoglycolate, and in so doing H_2O_2 is released by glycolate oxidase
186 in peroxisomes. It is therefore possible that rapid DAB staining in bundle sheath strands is
187 due to high rates of photorespiration in this cell type. To test this, we reduced the oxygen
188 tension to 2%, but found that this had no clear effect on DAB staining compared with controls
189 (Figure 3A&B). Moreover, when leaves of the C_4 species *Gynandropsis gynandra, Setaria*
190 *italica, Zea mays* and *Sorghum bicolor*, which generate up to tenfold higher concentrations
191 of CO_2 in bundle sheath cells and therefore minimal activities of photorespiration were
192 exposed to high light, DAB still accumulated in these cells over a similar time-course (Figure
193 3C). It therefore appears unlikely that preferential DAB staining in either C_3 or C_4 bundle
194 sheath cells is caused by H_2O_2 produced during photorespiration.

195 Taken together our results imply that accumulation of ROS in the bundle sheath of C_3
196 and C_4 plants is unlikely to be caused by limited capacity of the Calvin-Benson-Bassham
197 cycle compared with ability to harvest light energy. Furthermore, the data obtained by
198 suppressing photorespiration either transiently in C_3 leaves, or more permanently in C_4
199 leaves, are inconsistent with the notion that photorespiratory derived H_2O_2 is responsible for
200 the rapid accumulation of ROS in bundle sheath cells.

201

202 **Transcriptome profiling indicates balanced expression of photosynthesis genes but**
203 **elevated expression of genes encoding enzymes responsible for synthesis of reactive**
204 **oxygen species in bundle sheath strands**

205 To better understand the molecular basis for preferential accumulation of ROS in rice
206 bundle sheath strands we carried out RNA-SEQ on this tissue. Laser capture
207 microdissection was used to obtain mRNA from three biological replicates of bundle sheath
208 strands or mesophyll cells derived from leaves that had not received a high light treatment
209 (Figure 4A). Electropherograms showed that the RNA obtained was of good quality (Figure
210 4B). In total, over 165 million reads were generated using the Illumina sequencing platform.
211 For each replicate, on average about 78.5% of reads were mapped uniquely to the

212 Nipponbare reference genome (Supplemental Table 1). To enable comparison between
213 samples, we normalized all read counts with DESeq2, and to reduce noise, poorly
214 expressed genes with averaged normalized counts of < 10 in all samples were removed.
215 This led to a total of 15,727 genes being identified as expressed. Among these, 15456 genes
216 were expressed in both BSS and M cells, while 239 genes were only expressed in BSS and
217 32 genes only expressed in M cells (Figure 4C). Hierarchical clustering (Figure 4D) and
218 principal component analysis (PCA; Figure 4E) showed strong clustering between biological
219 replicates from each tissue. Indeed, the PCA showed that 92% of variance between
220 replicates was associated with one major component that mapped onto the tissue from
221 which RNA was isolated (Figure 4E). Using criteria of $\log_2$ fold change > 0.5 and an adjusted
222 *P* value < 0.05, we defined 3170 genes as being more highly expressed in bundle sheath
223 strands, and 2766 as more strongly expressed in mesophyll cells (Figure 4F).

224 We next analysed the abundance of transcripts derived from genes known to be
225 associated with the production of ROS. Specifically, we focused on genes encoding the
226 photosynthetic apparatus, and enzymes that either scavenge or synthesize ROS. In all
227 cases, to provide an overview of these complex processes eigengene values were
228 computed to take into account the fact that multiple genes encode these oligomeric protein
229 complexes. Transcripts encoding components of Photosystem II, Photosystem I, the
230 cytochrome b_6f complex, cyclic electron transport and the ATP synthase were less abundant
231 in bundle sheath strands compared with mesophyll cells (Figure 4G and Figure S3).
232 However, the mesophyll contains a larger chloroplast compartment (Kinsman and Pyke,
233 1998) and so this is to be expected. We thus normalized transcript abundance for each
234 complex to Photosystem II and Photosystem I (Figure S3). This showed that components of
235 Photosystem II, the cytochrome b6f complex and Photosystem I accumulated
236 stoichiometrically in both cell types (Figure 4G). In other words, there was no clear
237 imbalance in transcripts encoding one part of the photosynthetic electron transport chain
238 that might lead to impaired function. This was also true for transcripts encoding enzymes of
239 the Calvin-Benson-Bassham cycle (Figure 4G) indicating that the relative capacities of the
240 light-dependent reactions of photosynthesis and the Calvin-Benson-Bassham cycle are
241 balanced similarly in bundle sheath strands and mesophyll cells. These data are consistent
242 with our earlier finding that increasing the CO_2 concentration around leaves failed to abolish

243 accumulation of DAB staining in the rice bundle sheath (Figure 2A&B).

244 We also found no evidence from this analysis of transcript abundance that bundle sheath
245 strands have lower ability to detoxify ROS than the mesophyll (Figure 4H). After
246 normalization to transcripts for the Photosystems which would be an expected source of
247 ROS during high light stress, transcripts encoding enzymes known to scavenge ROS were
248 typically more abundant in bundle sheath strands compared with mesophyll cells (Figure
249 4H). However, transcripts encoding several NADPH-oxidase and superoxide dismutase
250 proteins, which generate superoxide and H_2O_2 respectively were more abundant in bundle
251 sheath strands compared with mesophyll cells (Figure 4I). In particular, transcripts encoding
252 RBOHA, RBOHC and RBOHI were considerably more abundant in bundles sheath strands
253 compared with mesophyll cells. Quantitative Polymerase Chain Reactions (Q-PCR)
254 confirmed these findings (Figure S4). These data imply that the rapid increase in ROS in
255 bundle sheath strands after exposure to high-light is unlikely associated with a limited ability
256 to dissipate energy associated with the photosynthetic electron chain, but rather appears
257 due to higher basal activities of proteins that synthesize ROS.

258

259 **NADPH-oxidase activity mediates the high light response in both green and etiolated**
260 **leaves**

261 To test whether NADPH-oxidase activity is important for ROS accumulation in bundle
262 sheath strands of rice we used inhibitors to block its activity, as well as a previously reported
263 overexpression line for the *OsRBOHA* gene that encodes the major RBOH isoform NADPH-
264 oxidase A in rice (Wang et al., 2016). Two commonly employed inhibitors of flavin-linked
265 enzymes, diphenyleneiodonium chloride (DPI) (O'Donnell et al., 1993) and imidazole (Iizuka
266 et al., 1985), were used to assess the role of NADPH oxidase. Both inhibitors reduced ROS
267 production in bundle sheath strands of rice after imposition of light stress (Figure 5A&B and
268 Figure S5A&B). The incomplete repression of ROS production associated with DPI or
269 imidazole treatment is consistent with some production being associated with
270 photosynthesis-related processes. To test whether this was the case, we next exposed
271 etiolated leaves that lack chlorophyll to high light in the absence or presence of each inhibitor.
272 Despite these leaves lacking chlorophyll, DAB staining was detected after exposure to high-
273 light (Figure 5C&D, Figure S5C&D). This is consistent with a significant amount of ROS

being produced from non-photosynthetic pathways. Moreover, in leaves lacking chlorophyll, inhibition of NADPH-oxidase activity completely abolished ROS production in bundle sheath strands (Figure 5C&D, Figure S5C&D). Q-PCR on RNA isolated from etiolated leaves confirmed that transcripts derived from *NADPH-oxidase A*, *NADPH-oxidase* C and *NADPH-oxidase I* genes as well as superoxide dismutase genes were more abundant in bundle sheath strands than in mesophyll cells (Figure S6). Whilst a mutant allele for *NADPH-oxidase B*, which was preferentially expressed in mesophyll cells (Figure 4I) had no impact on DAB staining during high light treatment (Figure S7), leaves from an overexpressor of *NADPH-oxidase A* (Wang et al., 2016) showed increased DAB staining in rice bundle sheath strands compared with controls (Figure 5E&F and Figure S8). We thus conclude that *NADPH-oxidase A* is important in mediating the response to high light in bundle sheath strands of rice.

286 **Discussion**

287 In the C_3 species *A. thaliana* it has been known for some time that bundle sheath cells
288 accumulate ROS in response to excess light (Fryer et al., 2002; Fryer et al., 2003;
289 Mullineaux et al., 2006; Galvez-Valdivieso et al., 2009). The work presented here shows that
290 a similar response is detected in bundle sheath strands of rice, a C_3 species from the
291 monocotyledons. Moreover, our analysis indicates that this phenomenon is not associated
292 with C_3 photosynthesis, but that it also takes place in bundle sheath strands from leaves of
293 C_4 plants. This was the case in C_4 *Gynandropsis gynandra*, which is sister to the
294 Brassicaceae, but also in the C_4 grasses maize, sorghum and *Setaria*. These findings imply
295 that the bundle sheath from dicotyledons and monocotyledons of both C_3 and C_4 species
296 fulfills a role in sensing and responding to excess light.

297 To better understand the causes for production of ROS in bundle sheath strands we used
298 rice. High light-induced ROS was not abolished by decreasing photorespiration in rice and
299 could be seen in the bundle sheath strands of C_4 species that lack photorespiration.
300 Therefore, photorespiratory H_2O_2 production in peroxisomes *via* glycolate oxidase is not
301 involved. The possibility that an imbalance between light harvesting and photosynthetic
302 electron transport and use of excitation energy by the Calvin-Benson-Bassham cycle in
303 bundle sheath cells was not supported by relative expression of genes encoding
304 photosynthetic components. After normalization, these have similar relative expression in
305 both cell types. This finding is consistent with analysis of the bundle sheath in C_3 *A. thaliana*
306 in which the photosynthetic apparatus is assembled and functional (Kinsman and Pyke,
307 1998; Janacek et al., 2009) despite lower levels of photosynthesis gene expression (Aubry
308 et al., 2014). We also failed to collect any convincing physiological evidence that ROS
309 production in the rice bundle sheath was associated with restricted activity of the Calvin-
310 Benson-Bassham cycle as might be expected if provision of CO_2 to this tissue distant from
311 stomata was limiting. The accumulation of ROS was neither accentuated nor ameliorated
312 when intercellular CO_2 concentrations were reduced or increased respectively.

313 In contrast to a purely photosynthetic origin of ROS in bundle sheath strands, we have
314 produced evidence that plasma membrane localized NADPH oxidase has a significant role.
315 NADPH oxidase catalyses extracellular reduction of oxygen, forming superoxide in the
316 apoplast. Membrane impermeable superoxide dismutates rapidly, producing H_2O_2 which is

317 proposed to enter the cytosol through aquaporins. NADPH oxidase has numerous isoforms
318 and is activated rapidly following numerous stimuli (Smirnoff and Arnaud, 2019). There is
319 evidence for apoplastic ROS production in *A. thaliana* bundle sheath cells in response to
320 high light (Galvez-Valdivieso et al., 2009) although NADPH depdendence was not
321 established. We found that three NADPH oxidase isoforms (RBOHA, RBOHC and RBOHI)
322 were more highly expressed in rice bundle sheath strands compared with mesophyll cells.
323 Consistent with NADPH oxidase being involved, application of the flavoprotein inhibitors
324 (DPI and imidazole) removed a large proportion of HL-induced ROS production. Moreover,
325 a mutant allele and overexpressing line for *OsRBOHB*, which was more abundant in
326 mesophyll cells showed no effect on ROS accumulation, whilst overexpression plants for
327 *OsRBOHA* led to increased production of ROS in the bundle sheath. Thus, differential
328 transcript abundance between the cell-types, pharmacological approaches to inhibit NADPH
329 oxidase activity, and genetic perturbation of the *OsRBOHA* locus supported the notion that
330 the bundle sheath strands have a greater ability than mesophyll cells to synthesize ROS in
331 response to high light. Furthermore, the observation that etiolated leaves have high light
332 induced ROS production provides key evidence that it is independent of photosynthesis and
333 supports a role for NADPH oxidase. How NADPH oxidase is activated by light in etiolated
334 leaves will need to be determined in the future. One possibility could be photoreceptor-
335 mediated NADPH oxidase activation. Cryptochrome generates superoxide upon exposure
336 to blue light and this has been proposed to contribute to part of its signaling role (El-Esawi
337 et al., 2017). However, it is also possible that photoreceptors could activate NADPH oxidase.
338 The results also suggest that part of the light-induced ROS derive from photosynthesis.
339 Given that previous work has shown that chloroplasts release H_2O_2 in the light and that this
340 could provide a high light signaling mechanism (Exposito-Rodriguez et al., 2017; Smirnoff
341 and Arnaud, 2019), the possible differences in the function of chloroplast and NADPH
342 oxidase-derived ROS requires investigation.

343 NADPH oxidase has previously been implicated in ROS responses induced by biotic and
344 abiotic stresses. In response to a localized stress event, an NADPH oxidase-dependent
345 ROS wave propagates between cells to initiate systemic responses in tissues distant from
346 the original stress (Miller et al., 2010; Mittler et al., 2011; Zandalinas and Mittler, 2018;
347 Fichman et al., 2019). Whilst we did not aim to investigate components underpinning such

348 a wave, or downstream responses, our findings have some relevance to the role of NADPH
349 oxidase in ROS production. The data imply that rice *RBOHA* plays a role in a local production
350 of ROS in bundle sheath strands. How these findings relate to previous work on *A. thaliana*
351 will require further work. The gene families encoding these proteins are large, and the
352 phylogenetic distance between *A. thaliana* and rice means that direct orthologs are not
353 always found, and function of these proteins may have diverged. However, *RBOHA* from
354 rice, which appears to play an important role ROS accumulation in the bundle sheath in
355 response to high light, is in the same orthogroup as *RBOHF* from *A. thaliana* (Figure S9A).
356 Interestingly, compared with the whole leaf, transcripts of *AtRBOHF* were more abundant in
357 bundle sheath cells (Figure S9B; (Aubry et al., 2014)). Thus, it is possible that these
358 orthologs fulfill similar functions in the bundle sheath strands of both species. However,
359 several lines of evidence point towards multiple pathways that both synthesize and
360 propagate ROS production in response to stresses. For example, analysis of *A. thaliana*
361 reported production of ROS in bundle sheath strands in leaves subjected to high light stress
362 (Fryer et al., 2002; Fryer et al., 2003; Mullineaux et al., 2006; Galvez-Valdivieso et al., 2009),
363 whilst in distant leaves ROS production is preferentially detected in mesophyll cells
364 (Fichman et al., 2019; Fichman and Mittler, 2020). Moreover, differential changes in stomatal
365 aperture of leaves subjected to stress compared with distant non-stressed leaves support a
366 model in which two different signals are involved in systemic stomatal responses. One that
367 is ABA based and associated with the vascular system (Schachtman and Goodger, 2008;
368 KangasjÄrvi et al., 2009; Gorecka et al., 2014; Yoshida and Fernie, 2018) and another that
369 uses ROS and travels through the plant (Devireddy et al., 2020). In fact, after a dark to light
370 transition in *A. thaliana*, local changes to stomatal aperture were not dependent on *RBOHD*,
371 but those changes associated with the systemic response were. *RBOHD* from *A. thaliana* is
372 orthologous to *RBOHI* from rice and in both species transcripts appear to be more abundant
373 in bundle sheath strands (Figure S9C&D and (Aubry et al., 2014)). This finding implies that
374 the role of these two proteins may have been conserved since they diverged from the last
375 common ancestor of rice and *A. thaliana*. Thus, downstream effects of production of ROS
376 in the bundle sheath will require additional experimentation. One important advance in this
377 area has been the ability to non-invasively monitor ROS either with reporters such as Hyper2
378 and roGFP (Exposito-Rodriguez et al., 2017; Nietzel et al., 2019), or with addition of

379 fluorescent dyes to intact leaves to allow time-course analysis in locally stressed as well as
380 distantly responding tissues (Fichman et al., 2019). Being able to apply these non-invasive
381 approaches to tissues such as the bundle sheath that are deep in the leaf and therefore
382 challenging to image will be informative in the future.

383 **Materials and methods**

384 **Plant materials and high light stress**

385 Rice (*Oryza sativa*. L) plants were grown for two weeks in compost in a growth chamber
386 with a 16 h photoperiod with a photosynthetic photon flux density (PPFD) of 75 µmol m^{-2} s^{-}
387 ^{1}, day night temperatures of 28 and 26°C respectively, and relative humility of 60%. In all
388 experiments, unless otherwise stated, IR64 was used. *OsRBOHA* and *OsRBOHB*
389 overexpression lines and *Osrbohb* mutants as well as their background (Nipponbare), were
390 grown under the same conditions. Etiolated plants were obtained by growing the plants in
391 compost in the dark at 28/26°C for 2 weeks.

392 In all cases, the middle part (~2.5 cm) of the second leaf was taken and infiltrated with
393 dye solution (see below). Leaves were then subjected to 750 µmol m^{-2} s^{-1}, which represented
394 a tenfold increase above that of growth. High light was provided using a Clark-type oxygen
395 electrode (LD2/3 oxygen electrode chamber) connected to an Oxylab control unit
396 (Hansatech Instruments Ltd., Norfolk, UK) and temperature maintained at 28°C using a
397 water tank. The top half of the leaves were illuminated by a liquid electronic display (LED)
398 light source (Hansatech LH36-2), whilst the bottom half of the leaf was covered with tin foil
399 to keep it in the dark.

400

401 **Chlorophyll fluorescence imaging**

402 Chlorophyll fluorescence measurements were performed using a chlorophyll fluorescent
403 imaging system (CF Imager, Technologica Ltd, Colchester, UK). ~ 2 cm leaf strips of the
404 middle part of second leaves were detached and floated on water in a 25-well square dish
405 and transferred immediately into the CF Imager. The application of pre-programmed
406 regimes of actinic growth light exposure times, dark periods, saturating light pulses, and the
407 calculation and imaging of the parameters F_v/F_m, F_q'/F_m', F_v'/F_m', and NPQ (Baker, 2008)
408 were performed using the manufacturers software-FluorImager.

409

410 **Detection of reactive oxygen species**

411 H_2O_2 production in the cells was detected by staining with 3,3'-diaminobenzidine
412 tetrachloride (DAB) (Fryer et al., 2002; Driever et al., 2009). The middle 2 cm from second
413 leaves were soaked in 5 mM DAB solution (pH 5.0) with 0.01% Tween-20. After shaking in

414 a dark incubator at 28°C for 2 hours, leaves were briefly dried with tissue paper, placed in a
415 Hansatech LD2/ 3 electrode leaf chamber and subjected to 750 μmol m^{-2} s^{-1}. Sampling was
416 undertaken at 0, 5, 10, 15, 20, 30, 40, 50, 60 mins. Prior to imaging, chlorophyll was removed
417 from the leaves by soaking in ethanol:acetic acid:glycerol (3:1:1) in a 70°C water bath for 1
418 hour, and then immersing in 70% (v/v) ethanol for 24 hours.

419 H_2O_2 production was also detected with 2',7'-dichlorodihydrofluorescein diacetate
420 (H_2DCFDA, Sigma-Aldrich). H_2DCFDA was dissolved in dimethyl sulfite (DMSO) to 20 mM,
421 and then diluted with H_2O to a final concentration of 10 μM for infiltration. Infiltration was
422 performed as previously described (Fryer et al., 2002; Driever et al., 2009). In short,
423 H_2DCFDA was fed through the transpiration stream under low light (20 μmol m^{-2} s^{-1}) for up
424 to 12 hours to ensure absorption throughout the leaf. After infiltration, leaves were then
425 clamped in the Hansatech LD2/3 electrode chamber and exposed to PPFD of 750 μmol m^{-}
426 ^{2} s^{-1} for 0, 30, 60 minutes. Prior to confocal laser scanning microscopy, the middle vein of
427 the leaf was imaged after generating a paradermal section by hand. To confirm whether
428 H_2DCFDA penetrated into the whole leaf, 30% (w/w) H_2O_2 solution was diluted to 100 mM
429 with 10 μM H_2DCFDA and used to infiltrate leaves under the same conditions as above.
430 Leaves infiltrated with ddH_2O at the same condition were used as controls. After infiltration,
431 green fluorescence was assessed by confocal laser scanning microscopy.

432 The NADPH oxidase inhibitors diphenyliodonium (DPI) and imidazole (Sigma) were
433 added to the DAB solution and infiltrated into leaves for 2 hours before high light treatment.
434 DPI chloride was dissolved in DMSO to 100 mM and then diluted to 100 μM with a 5 mM
435 DAB solution (pH 5.0, with 0.01% tween20). Imidazole was dissolved in DMSO to 1 mM and
436 then diluted with 5 mM DAB solution (pH 5.0, with 0.01% tween20) to 20 μM. To test the
437 effects of different CO_2 and O_2 contents on H_2O_2 products, DAB-infiltrated leaves were
438 subjected to the high light treatment as described above, using air mixtures with different
439 concentrations of CO_2 controlled by an open gas exchange analyzer (LI-6400, LI-COR
440 Biosciences, Lincoln, NE, USA) connected in line to the Hansatech LD2/ 3 electrode leaf
441 chamber. For measurements at 2% O_2 concentration, the LI-6400 air inlet was connected
442 to a gas cylinder with pre-mixed 2% O_2 in N_2.
443

444 **Paradermal sectioning of paraffin-embedded tissue**

445 Leaves used for paradermal sectioning had been treated with high light and chlorophyll
446 removed. Samples were cut into small pieces of ~ 5 mM and dehydrated in an ethanol series
447 consisting of 70% (v/v) for 30 minutes; 85% (v/v) for 30 minutes; 95% (v/v) for 30 minutes;
448 100% (v/v) ethanol twice for 30 minutes, then twice in 100% (v/v) Histo-Clear II for 60
449 minutes each, followed by two times in paraffin wax for 60 minutes at 60°C. Melted paraffin
450 wax was poured into 9-cm petri dishes and cut into small blocks once the wax was cool. For
451 paradermal sectioning, blocks were trimmed so that the surface of the leaf was parallel to
452 the surface of the block. 10 µm sections were obtained using a rotary microtome, floated in
453 a 60°C water bath and then mounted onto clean glass slides to dry overnight in an incubator
454 set at 42°C. Dehydration of the sections was performed as follows: 100% (v/v) Histo-Clear
455 II twice for 10 minutes each; 100% ethanol twice for 5 minutes each; 95% ethanol (v/v); 70%
456 (v/v) ethanol; 50% (v/v) ethanol; 30% (v/v) ethanol for 2 minutes each. Slides were then
457 rinsed with deionized H_2O; drained and then 30% (v/v) glycerol added prior to a coverslip.

458

459 **Laser capture microdissection**

460 For laser capture microdissection, leaf samples were cut into ~ 5 mm pieces and fixed in
461 100% (v/v) ice-cold acetone at 4°C for overnight. The next day, samples were dehydrated
462 and embedded with Steedman's polyester wax (Hua and Hibberd, 2019). Blocks were
463 sectioned using a rotary microtome to 8 µm thickness and then floated on Arcturus PEN
464 membrane slides (Fisher Scientific) with DEPC-treated water. The water was dried using
465 tissue paper and slides were stored at -20°C and used within 12 hours after sectioning. Prior
466 to LCM, slides were washed in 100% (v/v) ethanol for 5 mins and then air-dried for 5 mins.
467 LCM was performed using the ArcturusXT™ Laser Capture Microdissection System
468 (ThermoFisher) according to the manufacturer's instructions. Mesophyll cells and bundle
469 sheath stands were collected on the CapSure® Macro LCM Caps (ThermoFisher) and
470 immediately treated with extraction buffer (from Arcturus Picopure RNA extraction kit
471 (Thermo Fisher Scientific)) at 42°C for 30 minutes, then stored at -80°C.

472

473 **RNA extraction and quantitative PCR (qRT-PCR)**

474 Total RNA from LCM harvested mesophyll and bundle sheath cells was extracted using

475 Arcturus Picopure RNA extraction kit (ThermoFisher) with on-column DNaseI treatment
476 according to the manufacturer's protocol. cDNA synthesis for LCM samples was performed
477 using TruSeq RNA Library Preparation Kit v2 (RS-122-2001; Illumina). Total RNA from
478 whole leaves was extracted from 100 to 200 mg of fully expanded leaves using Triazol
479 reagent (Sigma-Aldrich) according to the manufacturer's instructions. Superscript II reverse
480 transcriptase (18064-022; ThermoFisher Scientific) was used for cDNA synthesis of whole
481 leaves. qRT–PCR was performed with the Bio-Rad CFX384 Real-Time PCR system using
482 the SYBR Green Jumpstart Taq ReadyMix (S4438-100RXN; Sigma-Aldrich) with the
483 following PCR conditions: 94°C for 5 mins and 40 cycles of 94°C for 10 s, 60°C for 1 min.
484 Relative gene expression levels were calculated using the $2^{-\Delta\Delta CT}$ method (Kubista et al.,
485 2006) and normalized with *OsUBQ5.* Gene-specific primer sequences are listed in
486 Supplemental Table 2. For each gene, three biological and three technical replicates were
487 performed.
488
489 **RNA-sequencing library preparation and data processing**
490 RNA integrity and quality of LCM samples were assessed using 2100-Bioanalyzer
491 (Agilent Technologies, USA) with an Agilent Bioanalyser RNA 6000 Pico assay and QuBit
492 (Thermo Fisher Scientific), respectively. Only samples RNA Integrity Number (RIN) ≥4.4
493 were selected for the final sample cohort. 50~150 ng starting total RNA from 12~15
494 paradermal sections of each replicate were used for RNA-seq library construction using the
495 QuantSeq 3' mRNA-Seq Library Prep Kit (Lexogen) according to the manufacturer's
496 recommendations. cDNA libraries were assessed using 2100-Bioanalyzer (Agilent
497 Technologies, USA) before 100 bp single-end sequencing using NextSeq500 (Illumina)
498 system at the Department of Biochemistry Sequencing Services at the University of
499 Cambridge based on standard protocols. Three biological replicates were conducted for
500 each cell type. Data processing was performed using custom scripts. Briefly, raw reads were
501 processed using Trimmomatic, mapped to the reference rice transcriptome genome
502 (MSU7.0, http://rice.plantbiology.msu.edu/index.shtml) and performed quantified using
503 Salmon (Patro et al., 2017). Differential expression analysis was performed using DESeq2.
504 Stringent criteria with $\log_2$ fold change ($\log_2$FC) >0.5 and adjusted p value (padj) < 0.05 were
505 used to screen the differentially expressed genes (DEGs) between bundle sheath strand

506 and mesophyll cells. Plots were generated with custom scripts in RStudio using the package
507 ggplot2. Three biological replicates for each cell type were performed.
508
509 **Generation of *OsRBOHB*-overexpression (*OsRBOHB*-OE) lines**
510 To generate the *OsRBOHB*-OE plants, the full-length coding region of *OsRBOHB* was
511 was amplified from the first-strand cDNA of Nipponbare and insert into vector pCAMBIA1301
512 under the control of ubiquitin promoter. The resulted construct was transformed into
513 Nipponbare by Agrobacterium-mediated transformation. The primers used for the construct
514 are listed in Supplemental Table 2.
515
516 **Imaging**
517 Intact leaves were imaged with Leica m165 FC microscopy. The paradermal sections
518 were imaged with Olympus BX41 microscopy. DAB staining intensity was quantified using
519 ImageJ (FIJI build, version 1.52q, NIH, USA). Confocal micrographs for detecting the DCF
520 fluorescence were taken using a Leica SP8 confocal microscopy (excitation 488 nm, barrier
521 515–555 nm).
522
523 **Statistical analysis**
524 All statistical analyses were conducted in R (v.3.6.3). Two-way analysis of variance
525 (ANOVA) was used to assess statistical differences in DAB staining between BSS and M
526 cells after a time course of high light treatment, and the effects of different concentrations of
527 CO_2 and O_2 concentrations on H_2O_2 production under high light treatment. Three-way
528 ANOVA was used for statistical analysis on the effects of different concentrations of CO_2 and
529 O_2 concentrations on H_2O_2 production under high light treatment and also used for assess
530 the data in experiments with the inhibitors DPI, imidazole, and also used to compare the
531 H_2O_2 production of *OsRBOHA*-OE and its wildtype under a time course of high light
532 treatment. Tukey Honest Significant Differences (TukeyHSD) test was performed for multiple
533 pairwise-comparison between the means of groups. Levene's test was used to check the
534 homogeneity of variances and Shapiro-Wilk test was used to check the normality
535 assumption. Unpaired T-tests were performed to compare differences in transcript
536 abundance between BSS and M cells and also used to compare the differences in DAB

537 staining between wild type and *OsRBOHB*-overexpression lines and mutants under
538 dark/high light conditions.
539
540 **Acknowledgements**
541 The work was funded by China International Postdoctoral Exchange Fellowship to HX, ERC
542 grant RG80867 Revolution to JMH and a C_4 Rice project grant from The Bill and Melinda
543 Gates Foundation to the University of Oxford (2015–2019).
544
545 **Competing interests**
546 The authors declare that they have no competing interests.

547 **References**

548 **Apel K, Hirt H** (2004) REACTIVE OXYGEN SPECIES: Metabolism, Oxidative Stress, and
549 Signal Transduction. Annu Rev Plant Biol **55**: 373–399

550 **Asada K** (1999) THE WATER-WATER CYCLE IN CHLOROPLASTS: Scavenging of Active
551 Oxygens and Dissipation of Excess Photons. Annu Rev Plant Physiol Plant Mol Biol **50**:
552 601–639

553 **Aubry S, Smith-Unna RD, Boursnell CM, Kopriva S, Hibberd JM** (2014) Transcript
554 residency on ribosomes reveals a key role for the Arabidopsis thaliana bundle sheath
555 in sulfur and glucosinolate metabolism. Plant J **78**: 659–673

556 **Baker NR** (2008) Chlorophyll fluorescence: a probe of photosynthesis in vivo. PG - 89-113
557 LID - 10.1146/annurev.arplant.59.032607.092759 [doi]. Annu Rev Plant Biol 89–11

558 **Bechtold U, Richard O, Zamboni A, Gapper C, Geisler M, Pogson B, Karpinski S,**
559 **Mullineaux PM** (2008) Impact of chloroplastic- and extracellular-sourced ROS on high
560 light-responsive gene expression in Arabidopsis. J Exp Bot **59**: 121–133

561 **Brown NJ, Palmer BG, Stanley S, Hajaji H, Janacek SH, Astley HM, Parsley K, Kajala**
562 **K, Quick WP, Trenkamp S, et al** (2010) C4 acid decarboxylases required for C4
563 photosynthesis are active in the mid-vein of the C3 species Arabidopsis thaliana, and
564 are important in sugar and amino acid metabolism. Plant J **61**: 122–133

565 **Crisp PA, Ganguly D, Smith AB, Murray KD, Estavillo GM, Searle IR, Ford E,**
566 **Bogdanović O, Lister R, Borevitz JO, et al** (2017) Rapid recovery gene
567 downregulation during excess-light stress and recovery in Arabidopsis. Plant Cell **29**:
568 tpc.00828.2016

569 **Demmig-Adams B, Adams WW** (1992) Responses of plants to high light stress. Annu Rev
570 Plant Physiol Plant Mol Biol **43**: 599–626

571 **Devireddy AR, Arbogast J, Mittler R** (2020) Coordinated and rapid whole-plant systemic
572 stomatal responses. New Phytol **225**: 21–25

573 **Devireddy AR, Zandalinas SI, Gómez-Cadenas A, Blumwald E, Mittler R** (2018)
574 Coordinating the overall stomatal response of plants: Rapid leaf-to-leaf
575 communication during light stress. Sci Signal. doi: 10.1126/scisignal.aam9514

576 **Dietz KJ** (2015) Efficient high light acclimation involves rapid processes at multiple
577 mechanistic levels. J Exp Bot **66**: 2401–2414

578 **Driever SM, Fryer MJ, Mullineaux PM, Baker NR** (2009) Imaging of reactive oxygen
579 species in vivo. Methods Mol Biol **479**: 109–116
580 **Dunand C, Crèvecoeur M, Penel C** (2007) Distribution of superoxide and hydrogen
581 peroxide in Arabidopsis root and their influence on root development: Possible
582 interaction with peroxidases. New Phytol **174**: 332–341
583 **El-Esawi M, Arthaut L-D, Jourdan N, d'Harlingue A, Link J, Martino CF, Ahmad M** (2017)
584 Blue-light induced biosynthesis of ROS contributes to the signaling mechanism of
585 Arabidopsis cryptochrome. Sci Rep **7**: 13875
586 **Exposito-Rodriguez M, Laissue PP, Yvon-Durocher G, Smirnoff N, Mullineaux PM**
587 (2017) Photosynthesis-dependent H2O2 transfer from chloroplasts to nuclei provides a
588 high-light signalling mechanism. Nat Commun **8**: 1–10
589 **Fichman Y, Miller G, Mittler R** (2019) Whole-Plant Live Imaging of Reactive Oxygen
590 Species. Mol Plant **12**: 1203–1210
591 **Fichman Y, Mittler R** (2020) Rapid systemic signaling during abiotic and biotic stresses: is
592 the ROS wave master of all trades? Plant J. doi: 10.1111/tpj.14685
593 **Fryer MJ, Ball L, Oxborough K, Karpinski S, Mullineaux PM, Baker NR** (2003) Control
594 of Ascorbate Peroxidase 2 expression by hydrogen peroxide and leaf water status
595 during excess light stress reveals a functional organisation of Arabidopsis leaves. Plant
596 J **33**: 691–705
597 **Fryer MJ, Oxborough K, Mullineaux PM, Baker NR** (2002) Imaging of photo-oxidative
598 stress responses in leaves. J Exp Bot **53**: 1249–1254
599 **Galvez-Valdivieso G, Fryer MJ, Lawson T, Slattery K, Truman W, Smirnoff N, Asami T,**
600 **Davies WJ, Jones AM, Baker NR, et al** (2009) The high light response in arabidopsis
601 involves ABA signaling between vascular and bundle sheath cells W. Plant Cell **21**:
602 2143–2162
603 **Gigolashvili T, Yatusevich R, Berger B, Müller C, Flügge U-I** (2007) The R2R3-MYB
604 transcription factor HAG1/MYB28 is a regulator of methionine-derived glucosinolate
605 biosynthesis in Arabidopsis thaliana. Plant J **51**: 247–261
606 **Gorecka M, Alvarez-Fernandez R, Slattery K, Mcausland L, Davey PA, Karpinski S,**
607 **Lawson T, Mullineaux PM** (2014) Abscisic acid signalling determines susceptibility of
608 bundle sheath cells to photoinhibition in high light-exposed Arabidopsis leaves. Philos

609 Trans R Soc B Biol Sci. doi: 10.1098/rstb.2013.0234
610 **Griffiths H, Weller G, Toy L, Dennis R** (2013) You're so vein: Bundle sheath physiology,
611 phylogeny and evolution in C3 and C4 plants. Plant Cell Environ **36**: 249–261
612 **Hatch MD** (1987) C4 photosynthesis: a unique elend of modified biochemistry, anatomy and
613 ultrastructure. Biochim Biophys Acta - Rev Bioenerg **895**: 81–106
614 **Hibberd JM, Quick WP** (2002) Characteristics of C4 photosynthesis in stems and petioles
615 of C3 flowering plants. Nature **415**: 451–454
616 **Hua L, Hibberd JM** (2019) An optimized protocol for isolation of high-quality RNA through
617 laser capture microdissection of leaf material. Plant direct **3**: e00156–e00156
618 **Iizuka T, Kanegasaki S, Makino R, Tanaka T, Ishimura Y** (1985) Pyridine and imidazole
619 reversibly inhibit the respiratory burst in porcine and human neutrophils: evidence for
620 the involvement of cytochrome b558 in the reaction. Biochem Biophys Res Commun
621 **130**: 621–626
622 **Janacek SH, Trenkamp S, Palmer B, Brown NJ, Parsley K, Stanley S, Astley HM, Rolfe**
623 **SA, Paul Quick W, Fernie AR, et al** (2009) Photosynthesis in cells around veins of the
624 C(3) plant Arabidopsis thaliana is important for both the shikimate pathway and leaf
625 senescence as well as contributing to plant fitness. Plant J **59**: 329–343
626 **KangasjÄrvi S, Nurmi M, Tikkanen M, Aro EM** (2009) Cell-specific mechanisms and
627 systemic signalling as emerging themes in light acclimation of C3 plants. Plant, Cell
628 Environ **32**: 1230–1240
629 **Kimura M, Yamamoto YY, Seki M, Sakurai T, Sato M, Abe T, Yoshida S, Manabe K,**
630 **Shinozaki K, Matsui M** (2003) Identification of Arabidopsis genes regulated by high
631 light-stress using cDNA microarray. Photochem Photobiol **77**: 226–233
632 **Kinsman EA, Pyke KA** (1998) Bundle sheath cells and cell-specific plastid development in
633 Arabidopsis leaves. Development **125**: 1815–1822
634 **Kleine T, Kindgren P, Benedict C, Hendrickson L, Strand A** (2007) Genome-Wide Gene
635 Expression Analysis Reveals a Critical Role for CRYPTOCHROME1 in the Response
636 of Arabidopsis to High Irradiance. Plant Physiol **144**: 1391–1406
637 **Koroleva OA, Gibson TM, Cramer R, Stain C** (2010) Glucosinolate-accumulating S-cells
638 in Arabidopsis leaves and flower stalks undergo programmed cell death at early stages
639 of differentiation. Plant J **64**: 456–469

640 **Leegood RC** (2008) Roles of the bundle sheath cells in leaves of C3 plants. J Exp Bot **59**:
641 1663–1673
642 **Li W, Zhu Z, Chern M, Yin J, Yang C, Ran L, Cheng M, He M, Wang K, Wang J, et al**
643 (2017) A Natural Allele of a Transcription Factor in Rice Confers Broad-Spectrum Blast
644 Resistance. Cell **170**: 114-126.e15
645 **Li Z, Wakao S, Fischer BB, Niyogi KK** (2009) Sensing and Responding to Excess Light.
646 Annu Rev Plant Biol **60**: 239–260
647 **Miller G, Suzuki N, Ciftci-Yilmaz S, Mittler R** (2010) Reactive oxygen species homeostasis
648 and signalling during drought and salinity stresses. Plant, Cell Environ **33**: 453–467
649 **Mittler R, Vanderauwera S, Suzuki N, Miller G, Tognetti VB, Vandepoele K, Gollery M,**
650 **Shulaev V, Van Breusegem F** (2011) ROS signaling: The new wave? Trends Plant Sci
651 **16**: 300–309
652 **Miyake H, Maeda E** (1976) Development of bundle sheath chloroplasts in rice seedlings.
653 Can J Bot **54**: 556–565
654 **Muller P** (2001) Non-Photochemical Quenching. A Response to Excess Light Energy. Plant
655 Physiol **125**: 1558–1566
656 **Mullineaux PM, Exposito-Rodriguez M, Laissue PP, Smirnoff N** (2018) ROS-dependent
657 signalling pathways in plants and algae exposed to high light: Comparisons with other
658 eukaryotes. Free Radic Biol Med **122**: 52–64
659 **Mullineaux PM, Karpinski S, Baker NR** (2006) Spatial dependence for hydrogen peroxide-
660 directed signaling in light-stressed plants. Plant Physiol **141**: 346–350
661 **Murchie EH, Niyogi KK** (2011) Manipulation of Photoprotection to Improve Plant
662 Photosynthesis. Plant Physiol **155**: 86–92
663 **Nietzel T, Elsässer M, Ruberti C, Steinbeck J, Ugalde JM, Fuchs P, Wagner S,**
664 **Ostermann L, Moseler A, Lemke P, et al** (2019) The fluorescent protein sensor
665 roGFP2-Orp1 monitors in vivo H(2) O(2) and thiol redox integration and elucidates
666 intracellular H(2) O(2) dynamics during elicitor-induced oxidative burst in Arabidopsis.
667 New Phytol **221**: 1649–1664
668 **Noctor G, Foyer CH** (1998) ASCORBATE AND GLUTATHIONE: Keeping Active Oxygen
669 Under Control. Annu Rev Plant Physiol Plant Mol Biol **49**: 249–279
670 **O'Donnell B V, Tew DG, Jones OT, England PJ** (1993) Studies on the inhibitory

671 mechanism of iodonium compounds with special reference to neutrophil NADPH
672 oxidase. Biochem J **290 (Pt 1**: 41–49
673 **Patro R, Duggal G, Love MI, Irizarry RA, Kingsford C** (2017) Salmon provides fast and
674 bias-aware quantification of transcript expression. Nat Methods **14**: 417–419
675 **Rossel JB, Wilson IW, Pogson BJ** (2002) Global Changes in Gene Expression in
676 Response to High. Society **130**: 1109–1120
677 **Ruban A V** (2016) Nonphotochemical Chlorophyll Fluorescence Quenching: Mechanism
678 and Effectiveness in Protecting Plants from Photodamage. Plant Physiol **170**: 1903–
679 1916
680 **Ruckle ME, Burgoon LD, Lawrence LA, Sinkler CA, Larkin RM** (2012) Plastids Are Major
681 Regulators of Light Signaling in Arabidopsis. Plant Physiol **159**: 366–390
682 **Sade N, Shatil-Cohen A, Attia Z, Maurel C, Boursiac Y, Kelly G, Granot D, Yaaran A,**
683 **Lerner S, Moshelion M** (2014) The Role of Plasma Membrane Aquaporins in
684 Regulating the Bundle Sheath-Mesophyll Continuum and Leaf Hydraulics. Plant Physiol
685 **166**: 1609 LP – 1620
686 **Sadey N, Shatil-Cohen A, Moshelion M** (2015) Bundle-sheath aquaporins play a role in
687 controlling Arabidopsis leaf hydraulic conductivity. Plant Signal Behav **10**: 1–4
688 **Sage RF** (2001) Environmental and Evolutionary Preconditionsfor the Origin and
689 Diversification of the C4 PhotosyntheticSyndrome. Plant Biol **3**: 202–213
690 **Schachtman DP, Goodger JQD** (2008) Chemical root to shoot signaling under drought.
691 Trends Plant Sci **13**: 281–287
692 **Shatil-Cohen A, Attia Z, Moshelion M** (2011) Bundle-sheath cell regulation of xylem-
693 mesophyll water transport via aquaporins under drought stress: a target of xylem-borne
694 ABA? Plant J **67**: 72–80
695 **Smirnoff N, Arnaud D** (2019) Hydrogen peroxide metabolism and functions in plants. New
696 Phytol **221**: 1197–1214
697 **Thordal-Christensen H, Zhang Z, Wei Y, Collinge DB** (1997) Subcellular localization of
698 H2O2 in plants. H2O2 accumulation in papillae and hypersensitive response during the
699 barley-powdery mildew interaction. Plant J **11**: 1187–1194
700 **Vogel MO, Moore M, Konig K, Pecher P, Alsharafa K, Lee J, Dietz K-J** (2014) Fast
701 Retrograde Signaling in Response to High Light Involves Metabolite Export, MITOGEN-

702 ACTIVATED PROTEIN KINASE6, and AP2/ERF Transcription Factors in Arabidopsis.
703 Plant Cell **26**: 1151–1165
704 **Wang X, Zhang M-M, Wang Y-J, Gao Y-T, Li R, Wang G-F, Li W-Q, Liu W-T, Chen K-M**
705 (2016) The plasma membrane NADPH oxidase OsRbohA plays a crucial role in
706 developmental regulation and drought-stress response in rice. Physiol Plant **156**: 421–
707 443
708 **Winterbourn CC** (2014) The challenges of using fluorescent probes to detect and quantify
709 specific reactive oxygen species in living cells. Biochim Biophys Acta **1840**: 730–738
710 **Yoshida T, Fernie AR** (2018) Remote Control of Transpiration via ABA. Trends Plant Sci **23**:
711 755–758
712 **Zandalinas SI, Mittler R** (2018) ROS-induced ROS release in plant and animal cells. Free
713 Radic Biol Med **122**: 21–27
714

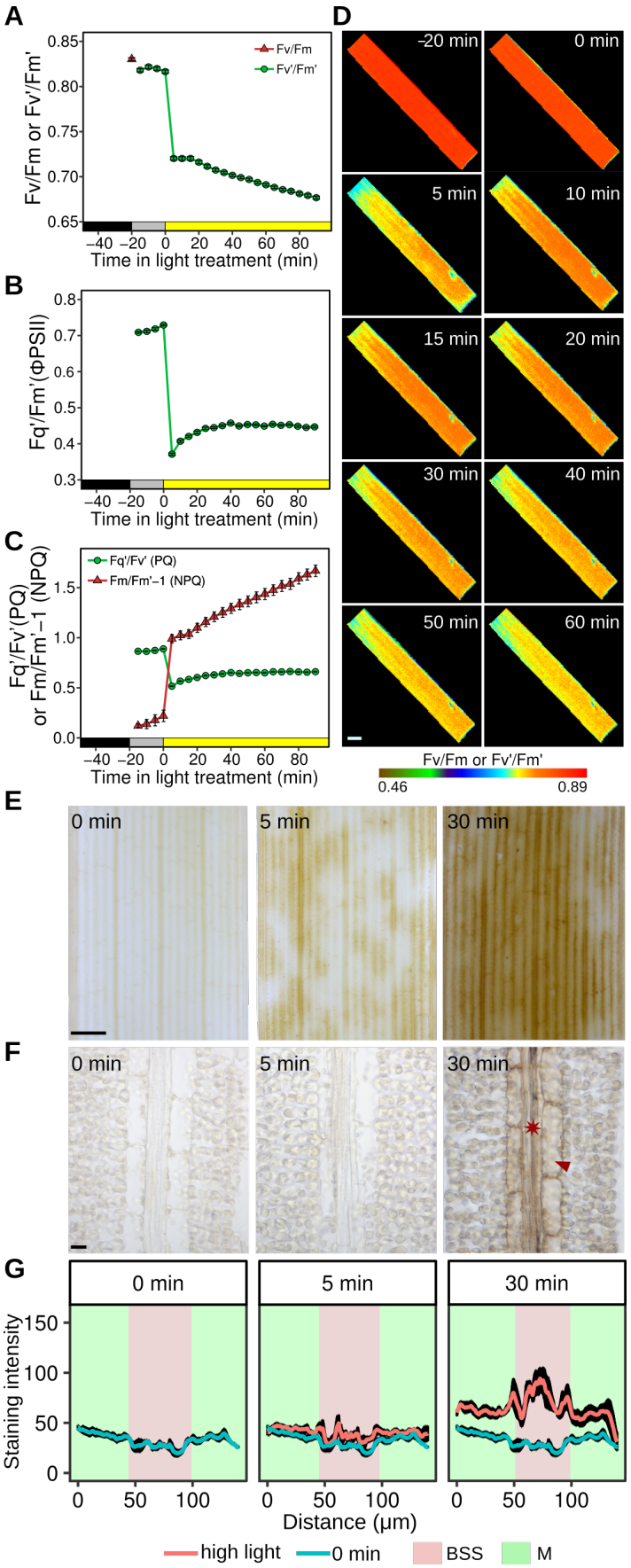

Figure 1. Rice bundle sheath strands preferentially accumulate the DAB polymerization product in response to high light. (A-C) Chlorophyll fluorescence parameters associated with dark-adapted leaves being moved into the light intensity of growth for 20 min, and then moved to a 10-fold higher intensity of light. (A) Dark-adapted F_v/F_m and F_v'/F_m' (B) Quantum efficiency of PSII (F_q'/F_m' or ΦPSII) and (C) Photochemical (PQ) and Non Photochemical Quenching (NPQ). Data shown represent mean and standard error from 16 leaves. (D) Representative images from the chlorophyll fluorescence imager showing responses were reasonably homogenous across the leaf. Scale bar = 2 mm. (E) High light stress led to strong staining from the DAB polymerization product in bundle sheath strands arranged along the proximal to distal axis of the leaf blade. After five minutes of high light staining is evident, but at thirty minutes it is stronger and more homogenous in these bundle sheath strands. Scale bar = 1 mm. (F) Representative image from paradermal sections show that cells accumulating DAB stain are veins (asterisk) and bundle sheath cells (arrowhead). Scale bar = 10 µm. (G) Quantitation of DAB stain in mesophyll and bundle sheath strands. Data are presented as mean (red or blue line) and one standard error from the mean, n= 4).

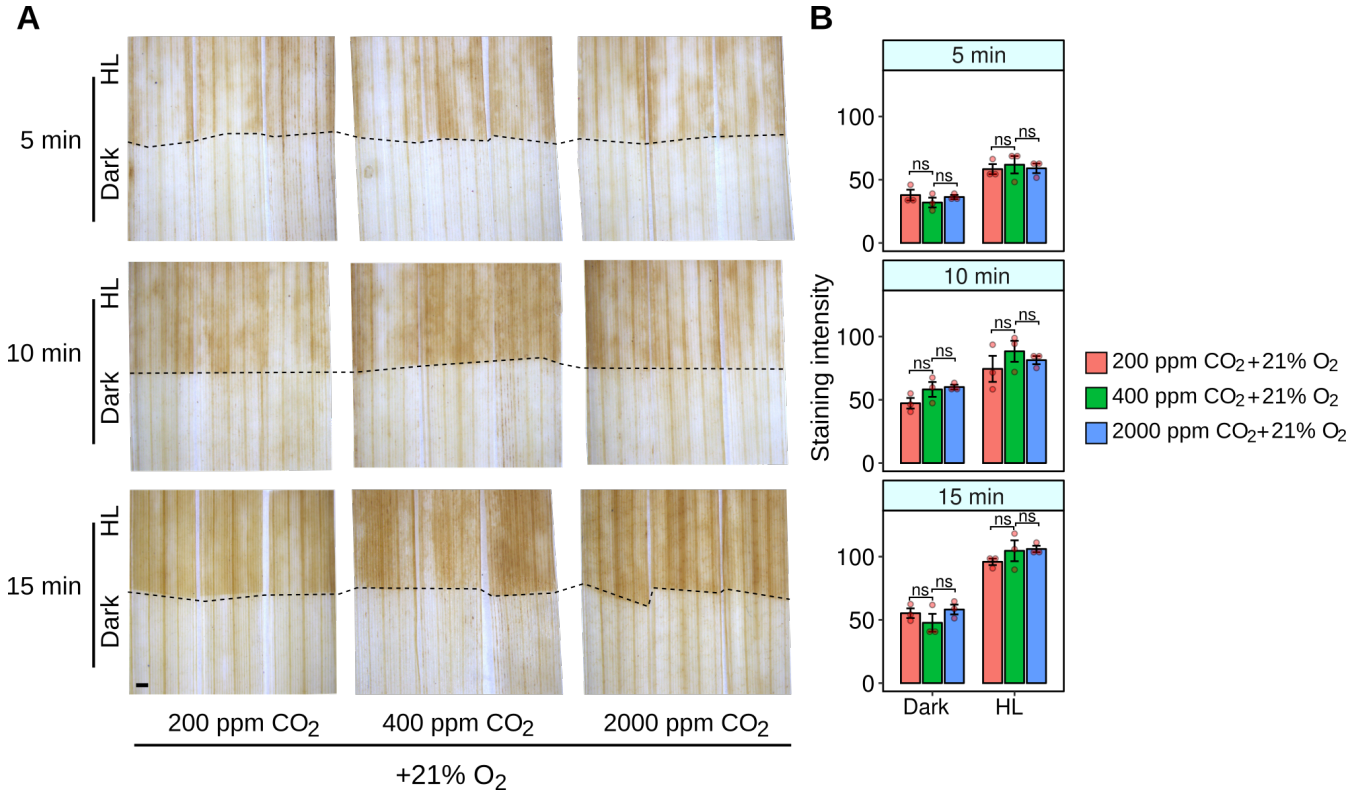

Figure 2. Altering CO_2 supply has little effect on the high light response of the rice bundle sheath. (A) Neither reducing (200 ppm) nor increasing (2000 ppm) CO_2 had a clear effect on DAB staining at 21% oxygen. (B) Quantitation of DAB staining of leaves subjected to low or high CO_2. ANOVA indicated no significant statistical difference associated with CO_2 treatment (p=0.22). Scale bar represents 1 mm.

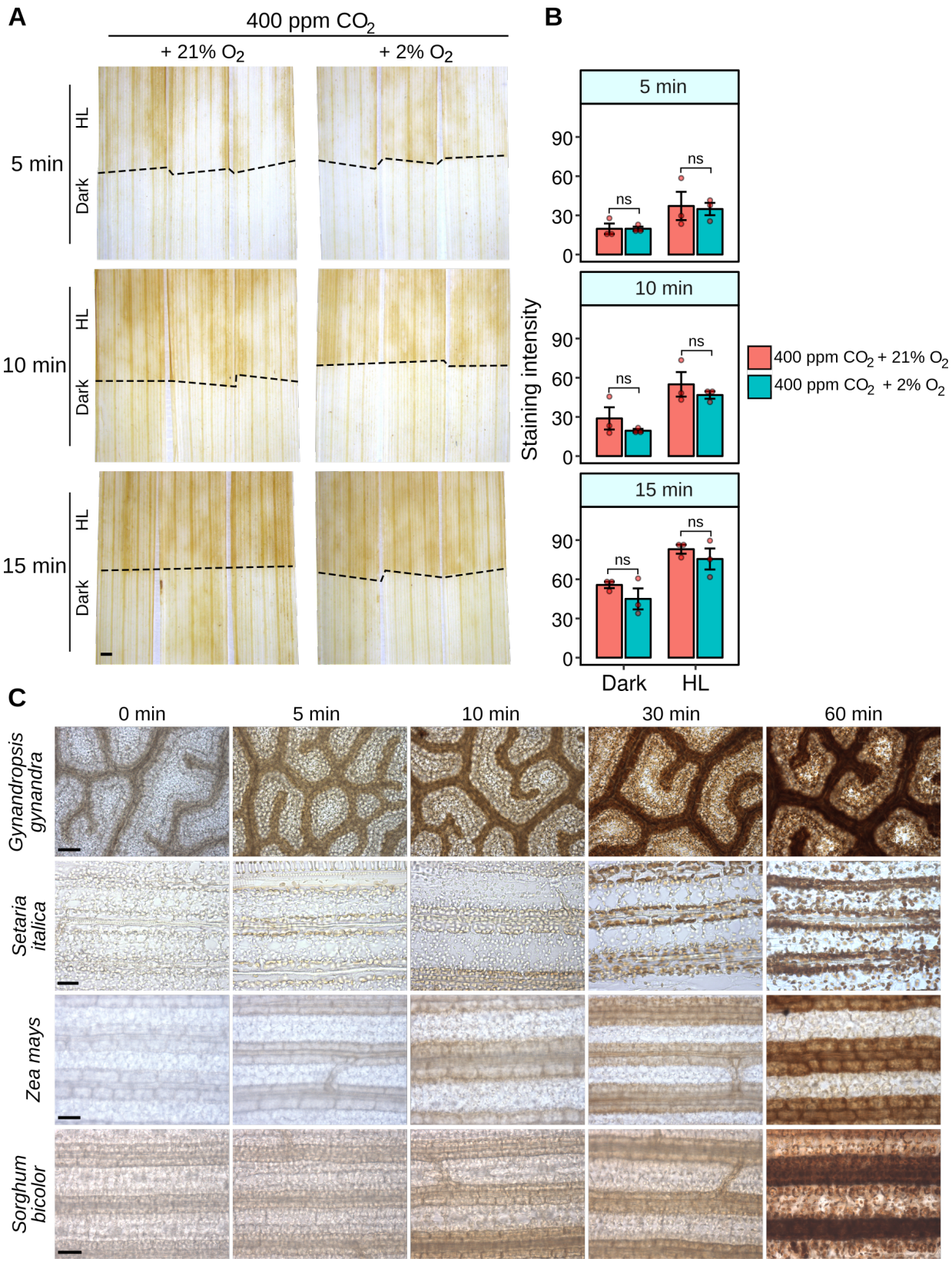

Figure 3. Photorespiration is not the source of the high light dependent accumulation of DAB stain in bundle sheath strands. (A) Representative images of DAB staining leaves exposed to 750 µmol m^{-2} sec^{-1} photon flux density for 5, 10 or 15 mins in 400 ppm CO_2 and either 21% or 2% O_2. Photorespiration is limited by 2% O_2. (B) Quantification of DAB staining. ANOVA indicated no significant statistical difference associated with O_2 treatment (p=0.0933). (C) DAB staining leaves of C_4 plants *Gynandropsis gynandra*, *Setaria italica, Zea mays, Sorghum bicolor* exposed to high light. Although C_4 plants have limited photorespiration in the bundle sheath, DAB staining was still detected in this tissue. Scale bars represent 1 mm (A) and 50 µm (B).

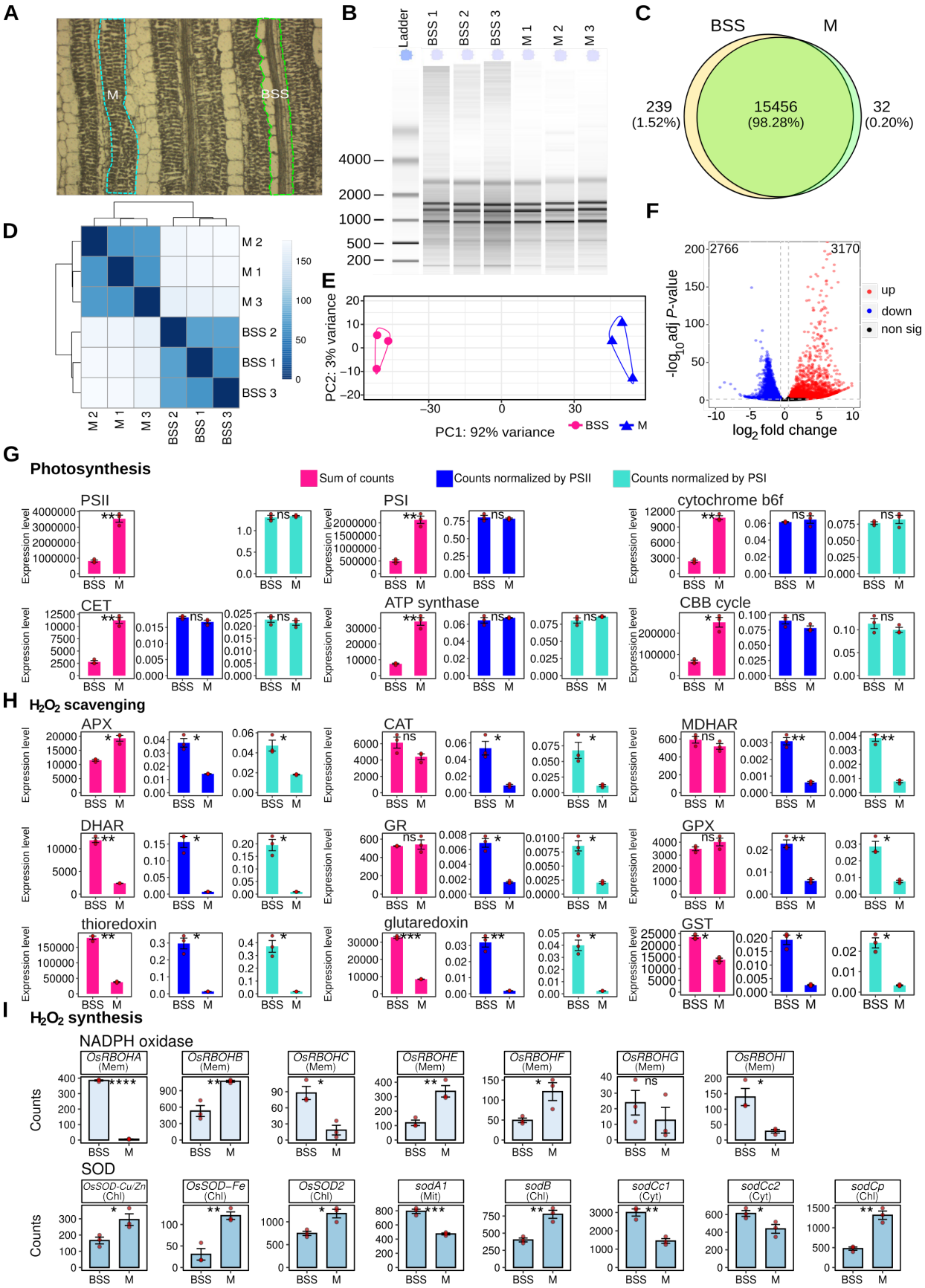

Figure 4. Global analysis mRNA from bundle sheath strands (BSS) and mesophyll (M) cells indicates balanced accumulation of transcripts encoding components of the photosynthetic electron transport chain and the Calvin Benson cycle, but that bundle sheath strands may have greater capacity to synthesise reactive oxygen species. (A) Bundle sheath strands (BSS) and mesophyll (M) were sampled for RNA using laser capture microdissection. (B) Electropherogram showing RNA quality. (C) Pie chart summarizing number of genes expressed in both BSS and M cells. (D) Hierarchical dendrogram and (E) Principal Component Analysis indicate that most variance was associated with tissue type. (F) Volcano plot showing number of differentially expressed genes between BSS and M. (G-I) Abundance of photosynthesis (G), H_2O_2 scavenging (H) and H_2O_2 synthesis (I) transcripts. For photosynthesis complexes the sum of all components of each complex is presented, and to take into account lower chloroplast content in bundle sheath strands these were normalized to either Photosystem I or II. Predicted subcellular localization of each NADPH oxidase (RBOH) and Superoxide dismutase (SOD) isoform is annotated (chl = chloroplast, mem = plasma membrane, mit = mitochondrial, cyt = cytoplasm.). T-tests indicate statistically significant differences (**** $p < 0.0001$, *** $p < 0.001$, ** $p < 0.01$, * $p < 0.05$).

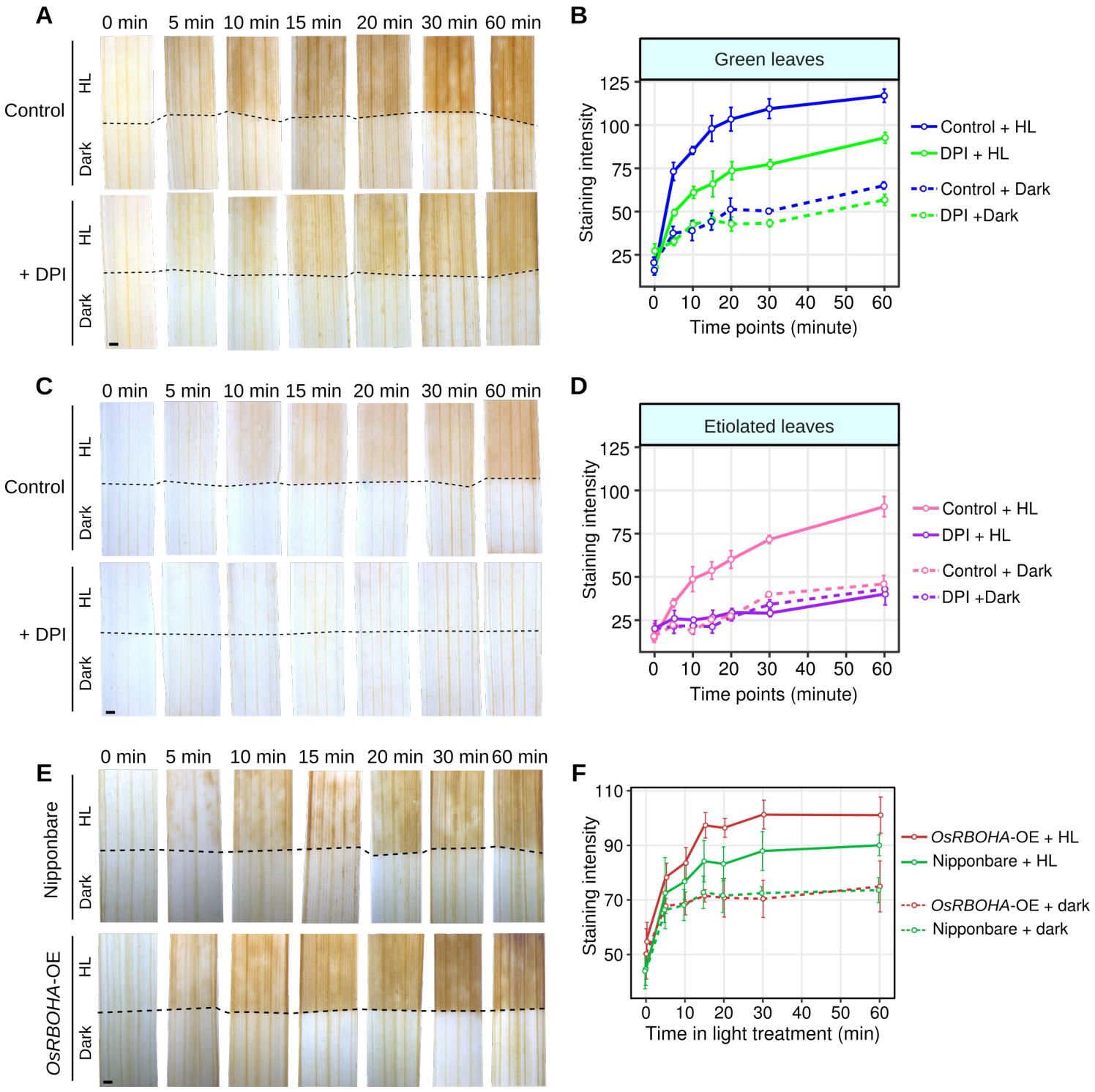

Figure 5. Inhibiting and increasing NADPH oxidase reduces and increases DAB staining respectively in bundle sheath strands of rice leaves. (A) Diphenyleneiodonium (DPI) a plasma membrane NAD(P)H oxidase inhibitor, partially inhibits DAB staining in bundle sheath strands of green leaves. (B) Quantitation of DAB staining over time in control compared with DPI and high light treated green leaves. (C) DPI completely inhibits DAB staining in etiolated leaves. (D) Quantitation of DAB staining over time in control and DPI high light treated etiolated leaves. (E) Overexpression of *OsRBOHA* increased DAB staining in bundle sheath strands after high light treatment. (F) Quantitation of DAB staining over time in green leaves from either the control or *OsRBOHA* overexpression line. In all cases the lower portion of the leaf (below the dotted line) was covered to provide an in-leaf control over the time-course. ANOVA showed DAB staining was reduced after DPI treatment in green leaves ($p<0.001$), etiolated leaves ($p<0.001$), and increased in *RBOHA* over-expressors ($p<0.05$). Scale bars represent 1 mm.

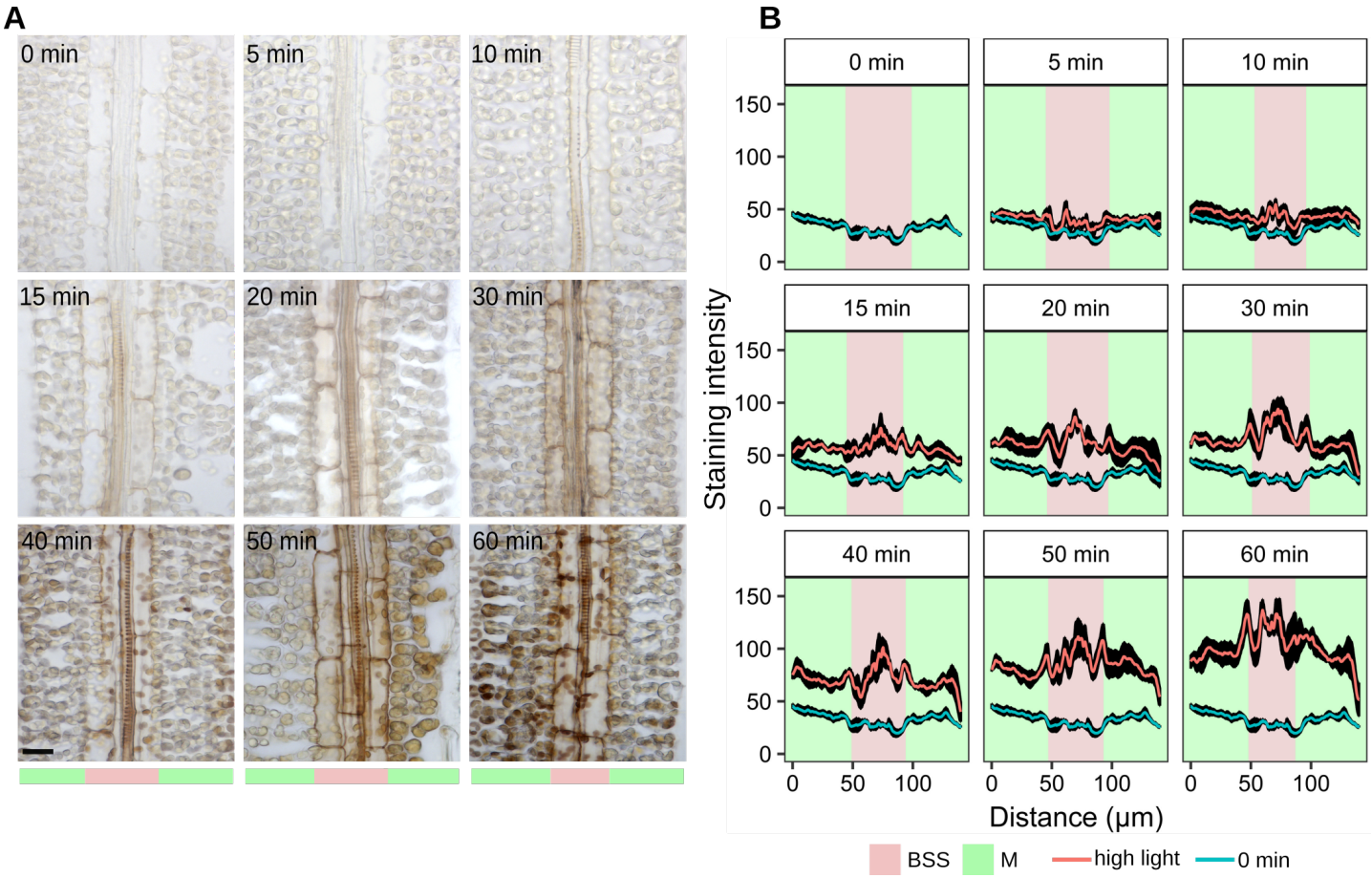

Figure S1. DAB staining of paradermal sections from rice leaves exposed to high light. (A) Representative images of leaves exposed to 750 µmol m^{-2} s^{-1} photon flux density for 0, 5, 10, 15, 20, 30, 40, 50 or 60 minutes. Brown stain indicates the formation of the polymerization product formed in the presence of reactive oxygen species. Scale bar denotes 10 µm. (B) Quantitation (arbitrary units) of DAB staining from paradermal sections illustrating the extent to which reactive oxygen species are first detected in vein and bundle sheath strands versus mesophyll cells The x-axis represents a scan from left to right across the paradermal sections. The y-axis depicts gray values extracted from paradermal sections. Data are presented as mean (red or blue line) and one standard error from the mean, n = 4). The response of bundle sheath strands to high light was greater than that of mesophyll cells (Two-way ANOVA $p < 0.001$).

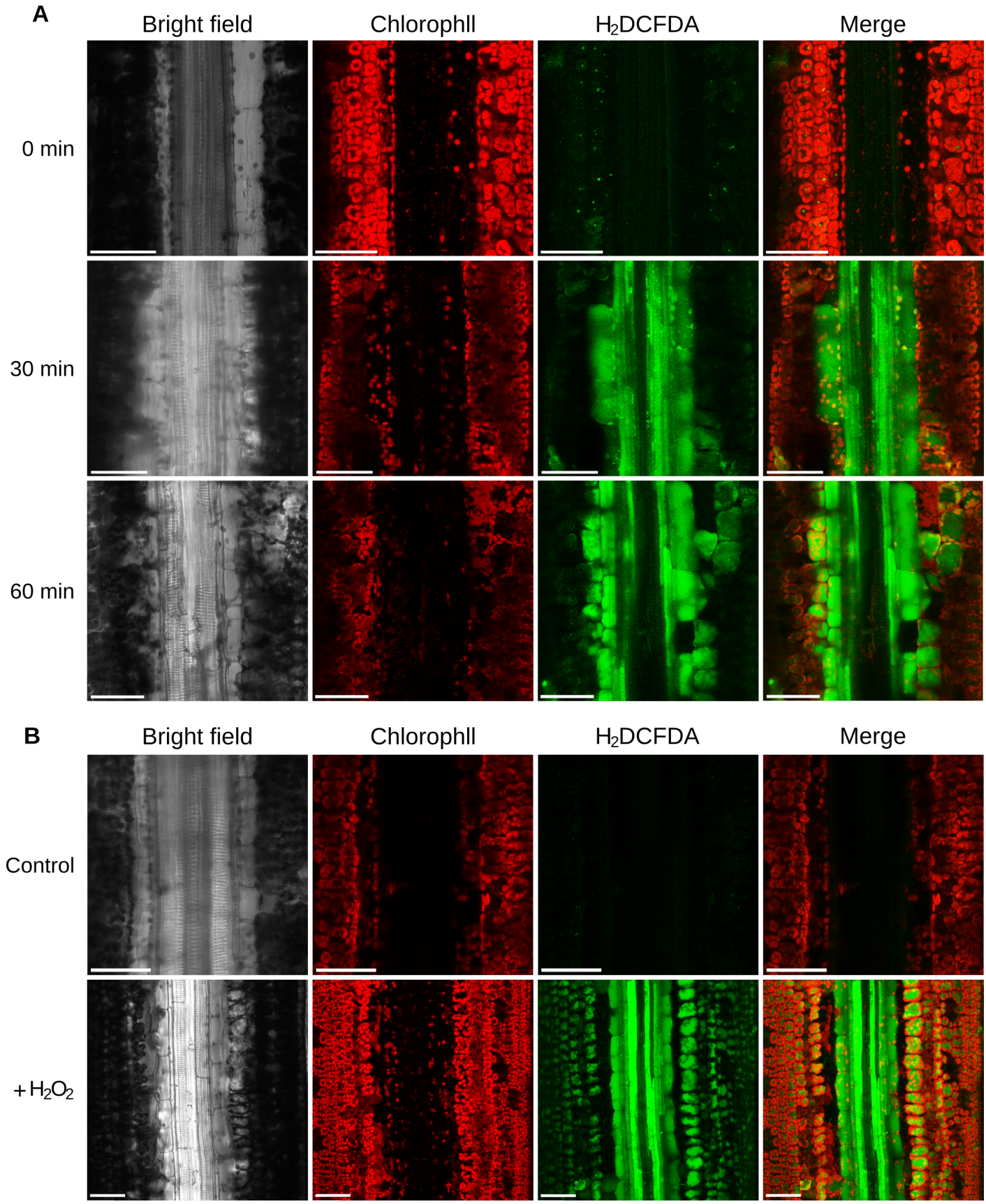

Figure S2. Confocal scanning microscopy indicates bundle sheath preferential fluorescence from H_2DCFDA in rice leaves exposed to high light. (A) Representative images of leaves were fed with 10 μM H_2DCFDA for 12 h prior to being exposed to high light (750 μmol m^{-2} s^{-1} photon flux density) for the times indicated. (B) Representative images from control leaves suppled with water as well as those suppled with 10 μM H_2DCFDA and exogenous 100 mM H_2O_2. Fluorescence from H_2DCFDA was not detected in control leaves, but in those to which H_2O_2 had been added it was detected in both mesophyll and bundle sheath strands. Scale bars denote 50 μm.

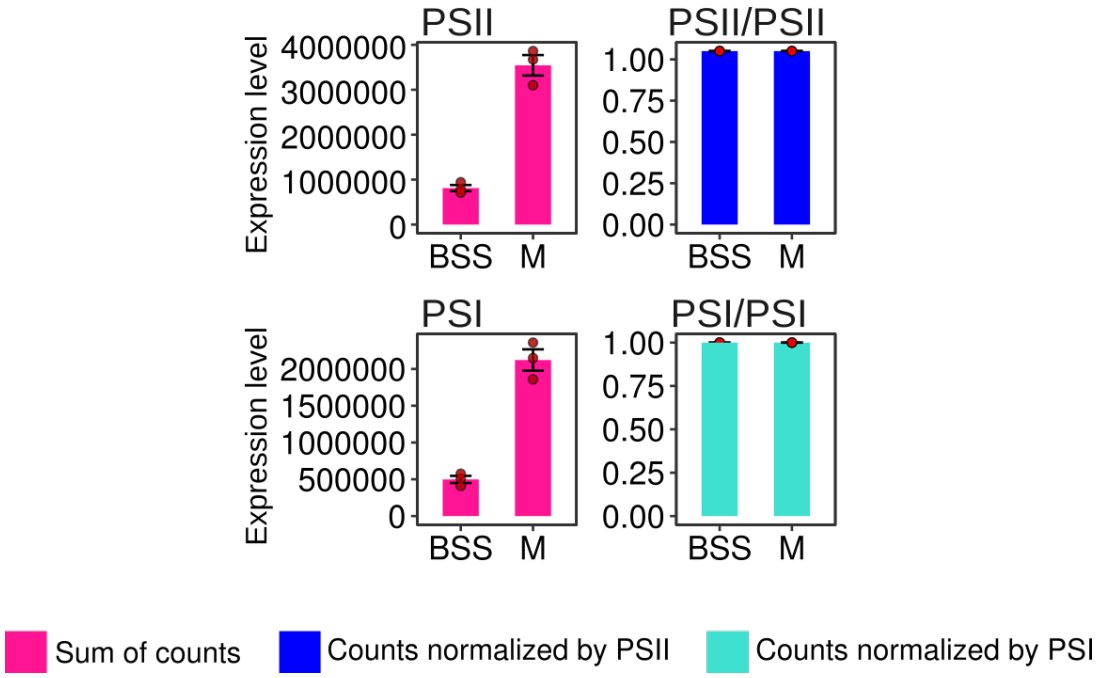

Figure S3. Normalisation of PSII and PSI against themselves indicates the expected one-to-one relationship.

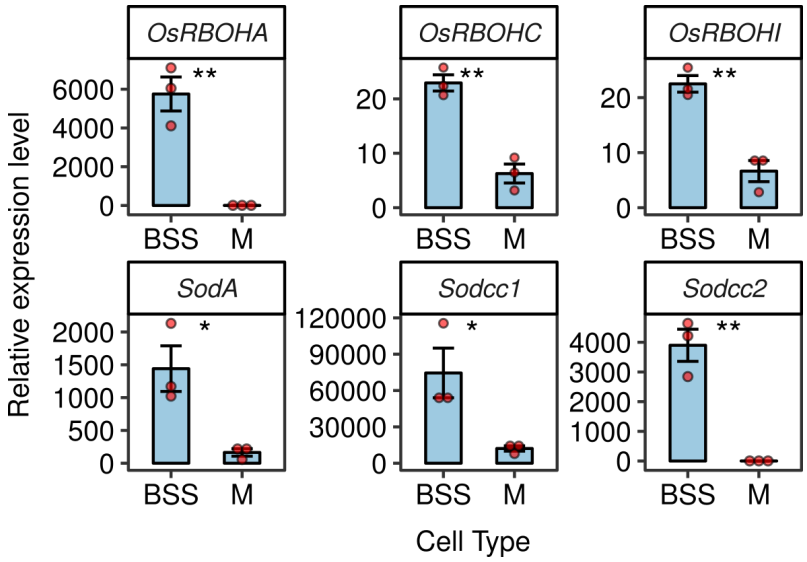

Figure S4. qPCR confirms analysis from deep sequencing and shows that transcripts of *RBOHA, RBOHC & RBOHI* as well as *SODA, SODCC1 & SODCC2* are more abundant in bundle sheath stands (BSS) than mesophyll (M) cells. RNA extracted from green leaves. Data are normalized to *OsUBQ5* as a control and presented as mean ± one standard error, n = 3. T-tests indicate statistically significant differences (** $p < 0.01$, * $p < 0.05$).

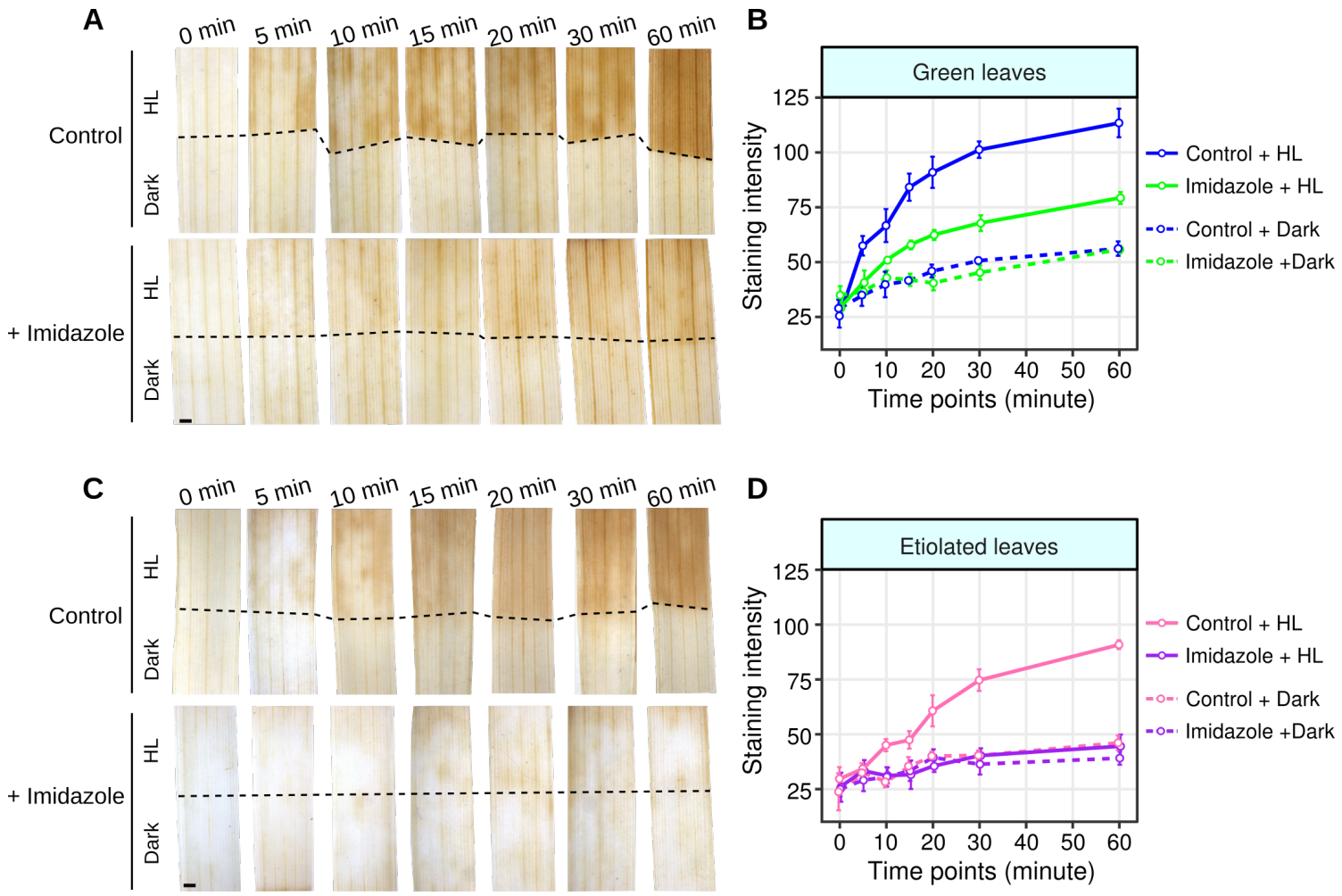

Figure S5. Inhibiting NAD(P)H oxidase activity with imidazole phenocopies the effect from diphenyleneiodonium in green and etiolated leaves. (A&B) Imidazole partially inhibits the accumulation of DAB in green leaves. (C&D) Imidazole completely inhibits DAB accumulation in etiolated leaves. ANOVA showed DAB staining was reduced after Imidazole treatment in green leaves ($p<0.001$), etiolated leaves ($p<0.001$).

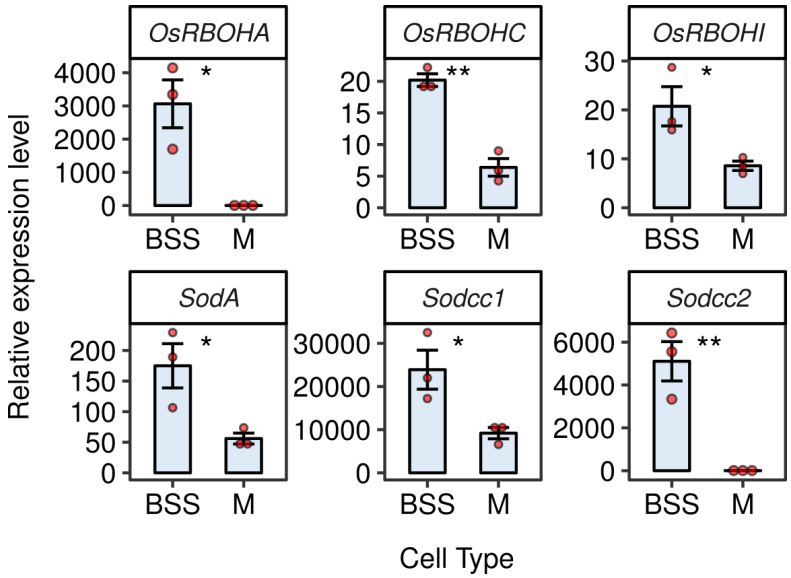

Figure S6. Q-PCR shows that transcripts encoding *OsRBOHA, RBOHC & RBPOHI* as well as *SODA, SODCC1 &SODCC2* are more abundant in bundle sheath strands than mesophyll ells in etiolated leaves of rice. *OsUBQ5* was used to normalize expression of each gene, and data are presented as the mean ± one standard error, n = 3. T-tests showed statistically significant difference between bundle sheath strands (BSS) and mesophyll (M) cells with ** = p< 0.01, * = p < 0.05.

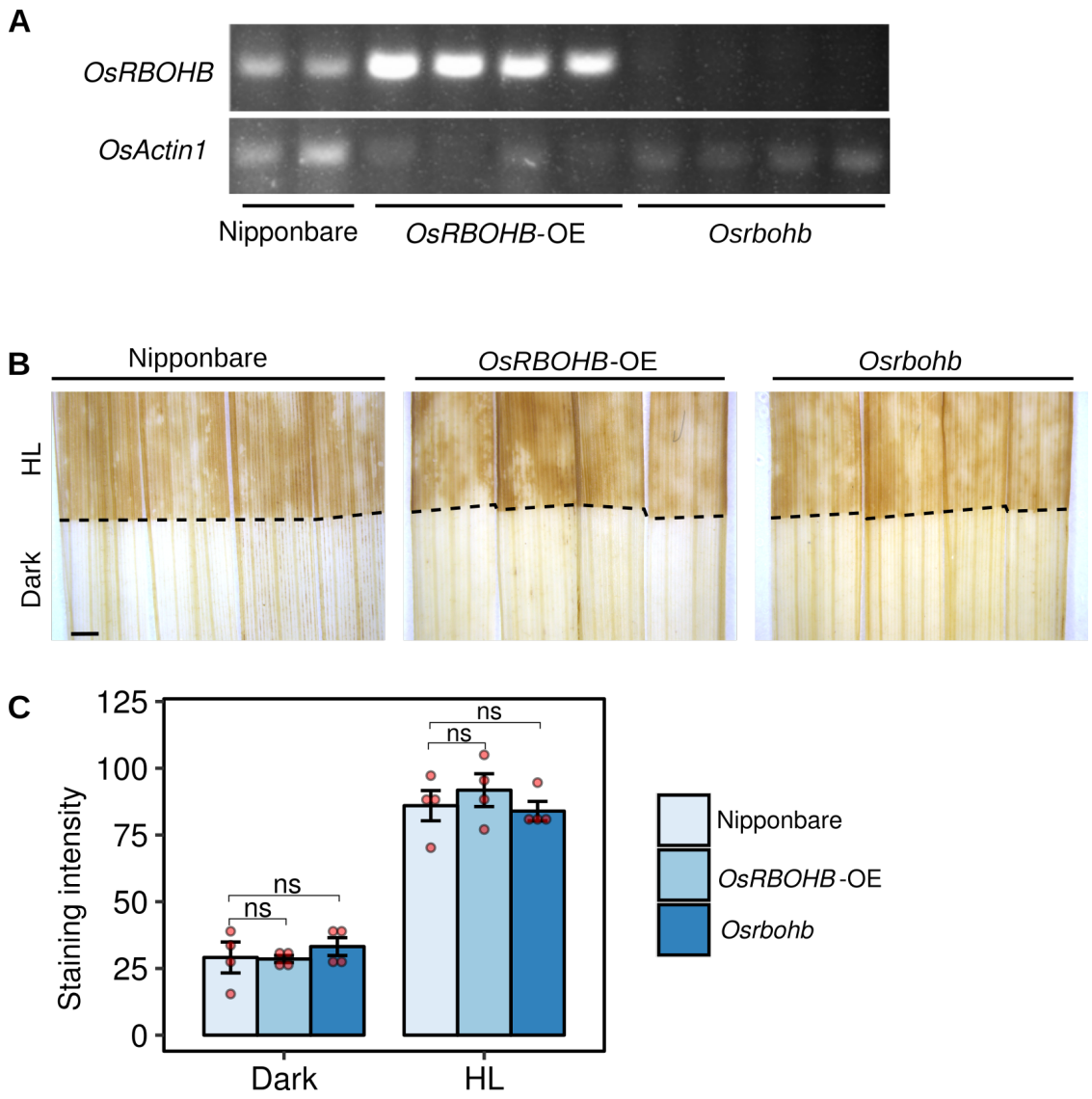

Figure S7. The *RBOHB* gene appears not to be involved in the high light response of the rice bundle sheath. (A) Semi-quantitative RT-PCR indicating that compared with the Nipponbare control, an over-expression line (*OsRBOHB-OE*) and a mutant allele (*Osrbohb*) contain increased and reduced transcripts from *RBOHB* respectively. *ACTIN1* is shown below as a control. (B) Representative images showing that the over-expression line and mutant allele of *RBOHB* show no difference in DAB staining compared with the Nipponbare control. (C) Quantification of DAB staining in (B). Scale bar represents 2 mm. T-tests showed that there was no significant (ns) statistical differences associated with over-expression of *OsRBOHB*.

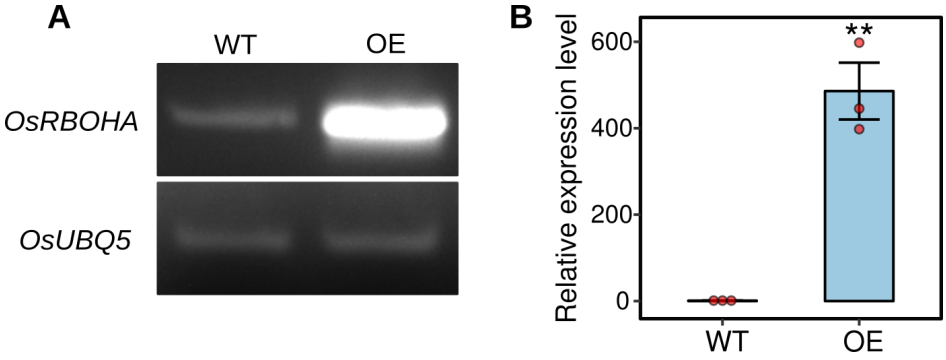

Figure S8. RT-PCR (A) and Q-PCR (B) were used to confirm over-expression of *OsRBOHA* compared with wild type (WT). *OsUBQ5* was used as a control. T-test showed statistically significant difference in the over-expressor (OE) compared with wild type (WT) ($p<0.01$).

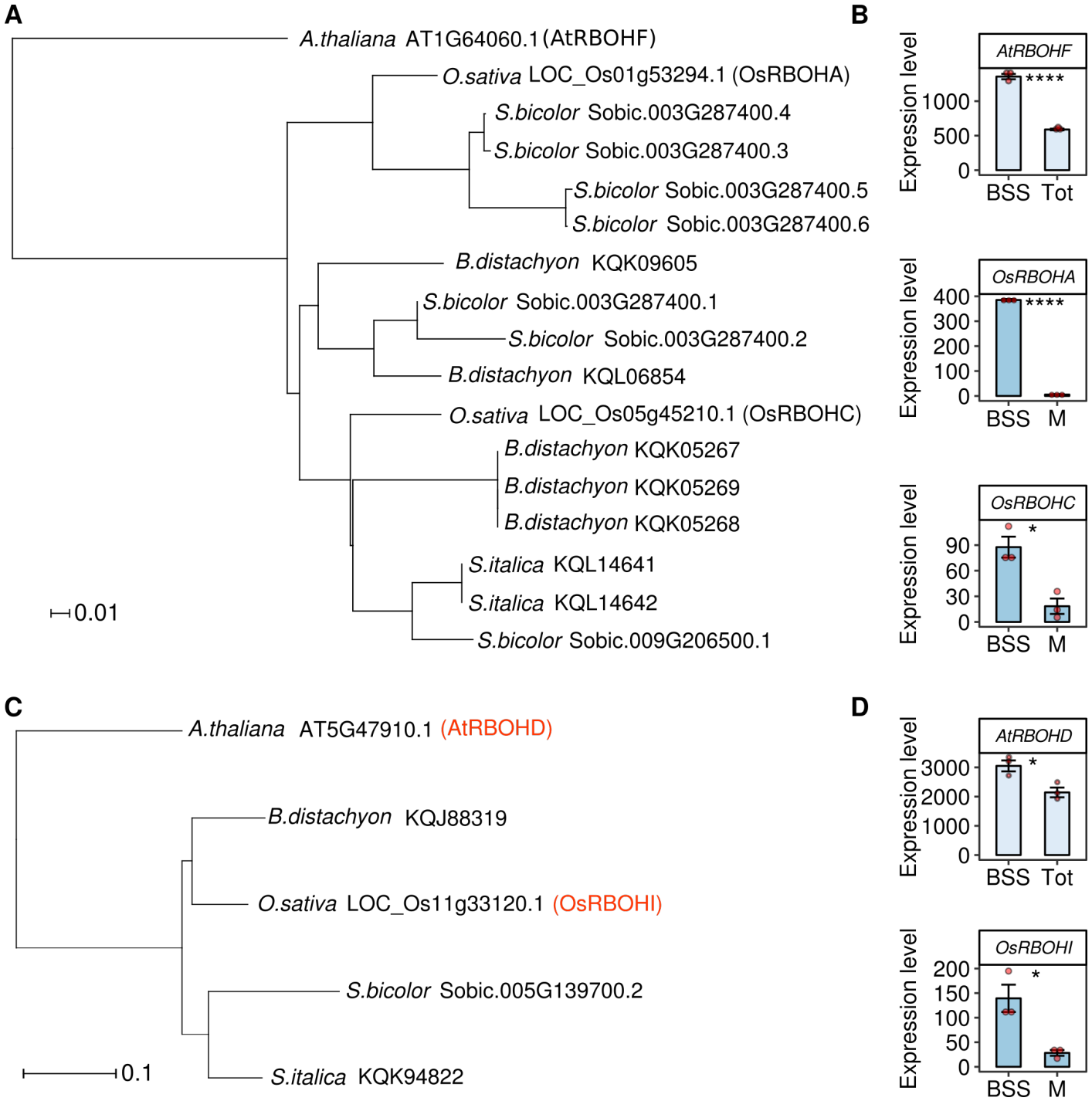

Figure S9. Phylogenetic reconstructions of *RBOH* genes depicting orthology relationships between those from rice, *Arabidopsis thaliana, Sorghum bicolor,* and *Brachypodium distachyon*. (A) Phylogenetic reconstruction indicating likely relationship between *AtRBOHF* and related genes in the grasses. (B) Transcript abundance of *AtRBOHF* in bundle sheath strands and total leaf material of *A. thaliana,* and of *OsRBOHA* and *OsRBOHC* in bundle sheath strands and mesophyll cells of rice. (C) Phylogenetic reconstruction indicating likely relationship between *AtRBOHD* and related genes in the grasses. *AtRBOHD* and *OsRBOHI* are highlighted in red. (D) Transcript abundance of *AtRBOHD* in bundle sheath strands and total leaf material or *A. thaliana* and of *OsRBOHI* in bundle sheath strands and mesophyll cells of rice. T-tests show statistically significant differences between cell type **** = $p < 0.0001$, * = $p < 0.05$.